Bioorganic Chemistry 144 (2024) 107164

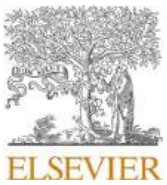

Contents lists available at ScienceDirect

Bioorganic Chemistry

journal homepage: www.elsevier.com/locate/bioorg

Discovery of a septin-4 covalent binder with antimetastatic activity in a mouse model of melanoma

Federica Blua [a,1], Chiara Monge [a,1], Simone Gastaldi [a,1], Nausicaa Clemente [b], Stefania Pizzimenti [c], Loretta Lazzarato [a], Rebecca Senetta [d], Serena Vittorio [e], Casimiro Luca Gigliotti [f], Elena Boggio [f], Umberto Dianzani [f], Giulio Vistoli [e], Alessandra Anna Altomare [e,*], Giancarlo Aldini [e], Chiara Dianzani [a,*], Elisabetta Marini [a,*], Massimo Bertinaria [a]

[a] Department of Drug Science and Technology, University of Turin, Turin, Italy
[b] Settore Centri di Ricerca e Infrastrutture di Ateneo e Laboratori - Polo di NO, University of Piemonte Orientale, Novara, Italy
[c] Department of Clinical and Biological Science, University of Turin, Torino, Italy
[d] Department of Medical Sciences, University of Turin, Turin, Italy
[e] Department of Pharmaceutical Sciences, University of Milan, Milan, Italy
[f] Department of Health Sciences, University of Piemonte Orientale, Novara, Italy

ARTICLE INFO

Keywords:
Cancer dissemination
Anti-metastatic agents
Invasiveness inhibition
Septin-4
Peptide mapping

ABSTRACT

Cancer spreading through metastatic processes is one of the major causes of tumour-related mortality. Metastasis is a complex phenomenon which involves multiple pathways ranging from cell metabolic alterations to changes in the biophysical phenotype of cells and tissues. In the search for new effective anti-metastatic agents, we modulated the chemical structure of the lead compound AA6, in order to find the structural determinants of activity, and to identify the cellular target responsible of the downstream anti-metastatic effects observed. New compounds synthesized were able to inhibit *in vitro* B16-F10 melanoma cell invasiveness, and one selected compound, CM365, showed *in vivo* anti-metastatic effects in a lung metastasis mouse model of melanoma. Septin-4 was identified as the most likely molecular target responsible for these effects. This study showed that CM365 is a promising molecule for metastasis prevention, remarkably effective alone or co-administered with drugs normally used in cancer therapy, such as paclitaxel.

1. Introduction

Although significant improvement in both early diagnosis and treatment of cancer patients, the hallmark ability of tumor cells to disseminate to distant organs in the body generating metastasis [1] is still the major cause of cancer-related deaths [2]. In patients, a large number of cancer cells is released in the blood circulation daily; nonetheless, metastasis formation itself is a rare event because cancer cells need to overcome multiple environmental obstacles before they can reach the blood and then extravasate and grow in other organs [3]. Indeed, cancer cells need to be able to continuously adapt to changing environments during metastasis, thus only very few metastatic cancer cells with the appropriate adaptations will colonize at distant sites [4,5].

Despite metastasis being the key cause of failure of cancer therapy and mortality, it remains a complex and not fully understood phenomenon. This process involves activation and inactivation of specific genes, a number of growth factors [6] and signaling pathways [7], which together trigger the epithelial–mesenchymal transition (EMT), i.e. the *trans*-differentiation process through which transformed epithelial cells develop the ability to invade, resist stress, and disseminate [8]. Moreover, it is recognized that the metastatization process also involves changes in the metabolic profile of cancer cells [3], and in the biophysical phenotype of cells and tissues, such as the adhesive force mechanics responsible for both cell–cell and cell-extracellular matrix (ECM) interactions [9].

Unlike primary tumors, which can often be cured using local surgery

* Corresponding authors.
E-mail address: elisabetta.marini@unito.it (E. Marini).
[1] These authors equally contributed to the work.

https://doi.org/10.1016/j.bioorg.2024.107164
Received 6 December 2023; Received in revised form 23 January 2024; Accepted 28 January 2024
Available online 29 January 2024

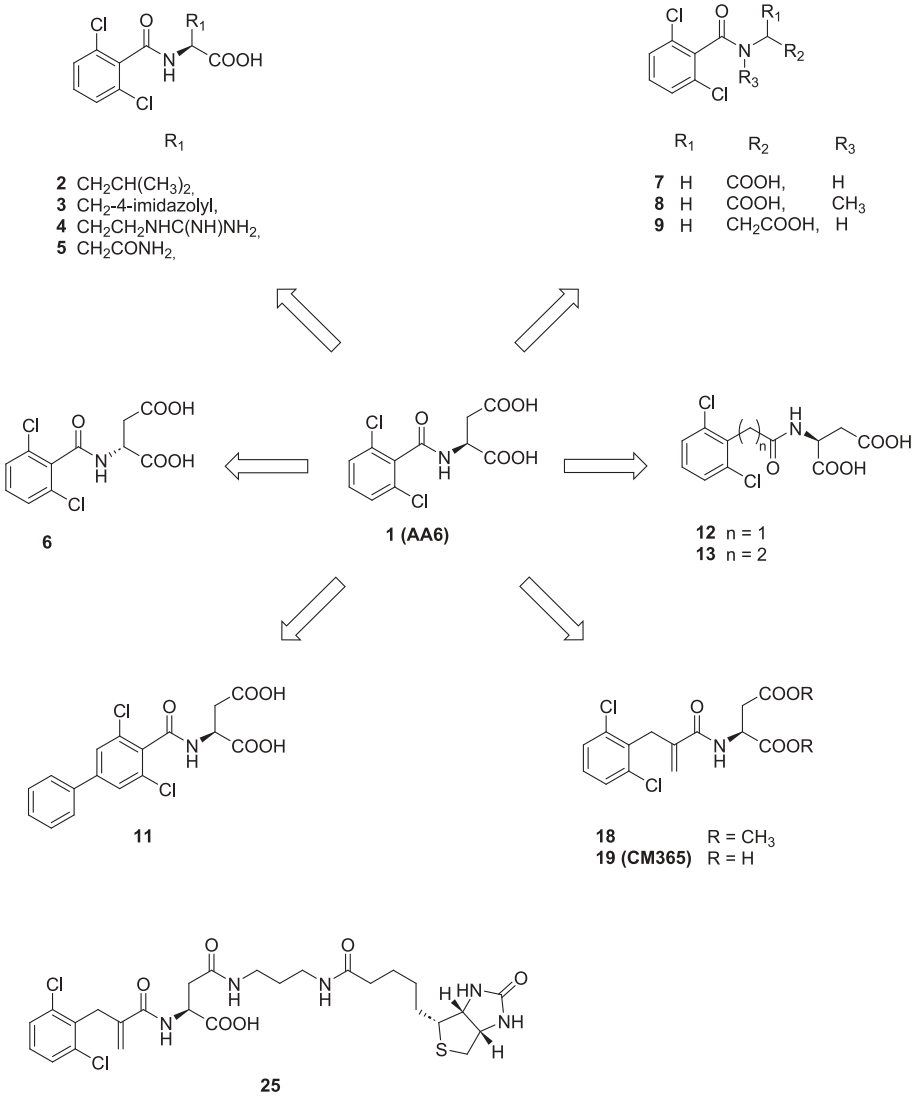

Fig. 1. Structure of AA6 and newly synthesized AA6 derivatives herein studied. The structures of the synthetic intermediates **10**, **14**–**17** and **20**–**24** are reported in schemes 3, 4 and 5 respectively.

and radiation, metastasis can be considered a systemic disease. Systemic approaches, including screening, chemotherapy, targeted therapy and immunotherapy, are therefore the mainstay of metastasis prevention and treatment [10]. Given the need of effective anti-metastatic therapies, in a previous work we studied a novel compound, the (S)-2-[(2,6-dichlorobenzoyl)amino] succinic acid (AA6, compound **1** in Fig. 1), as potential anti-metastatic drug in a spontaneous lung metastasis mouse model of breast cancer [11].

Metabolic alterations [12,13], inefficient DNA demethylation [14,15], cell–cell interactions mediated by adhesion proteins [16,17], and intracellular cytoskeleton remodulation [18] have been well defined as crucial steps along metastatic progression. In this context, AA6 was identified as a promising antimetastatic agent since it was able to prevent lung metastasis formation in the 4 T1 mouse model of breast cancer [19].

On this basis, we designed and synthesized a new series of compounds in order to obtain more effective anti-metastatic agents. The structure of the lead compound AA6 (**1**) was modulated in order to find the structural determinants of the anti-metastatic effect (Fig. 1).

We modified: (i) the aspartic acid moiety (compounds **2**–**9**), (ii) the steric hindrance of the substituted benzene ring (compound **11**), (iii) the distance between the benzene ring and the amide group (compounds **12**, **13**, **18** and **19**).

Since malignant melanoma is a highly aggressive tumor, able to disseminate from a relatively small primary lesion and metastasize to multiple sites, including the lung, brain, bone, liver, and lymph nodes [20], the new compounds were first investigated as inhibitors of *in vitro* B16-F10 melanoma cell invasiveness and adhesion to MS1endothelial cells, two well-known initial steps of metastasis [21].

Moreover, compounds **19** (CM365) and **25**, analogues of AA6 bearing a reactive double bond were synthesized. Thanks to the acrylamide Michael acceptor warhead, these compounds are potentially able to afford covalent binding to the target [22–24]; thus, they were used to identify the molecular target responsible for the downstream anti-metastatic effects observed. Finally, the effects of *in vivo* treatment with CM365 in a lung metastasis mouse model of melanoma are here reported.

2. Materials and methods

2.1. Reagents

Formic acid (FA), trifluoroacetic acid (TFA) and acetonitrile (ACN) were LC-MS grade. Ultrapure water was prepared by a Milli-Q

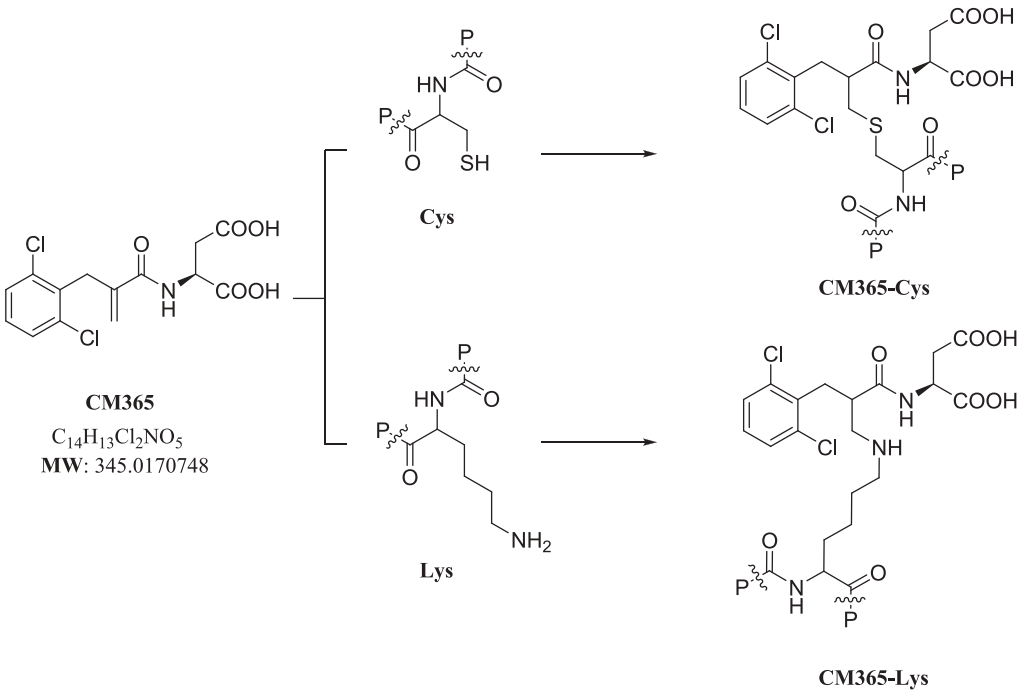

Scheme 1. Structural formulae of predicted CM365 covalent adducts with nucleophilic residues in membrane proteins (cysteine and lysine) to be investigated.

purification system (Millipore, Bedford, MA, USA).

Bradford Reagent, Any K_D ™ Mini Protean® TGX ™ precast gel, Standard Precision Plus pre-stained protein standards, Laemmli sample buffer, Running buffer and Bio-Safe Coomassie, together with the *threo*-1,4-Dimercapto-2,3-butanediol (DTT) and iodoacetamide (IAA) were supplied by Bio-Rad Laboratories, Inc. Trypsin was purchased from Roche Diagnostics SpA (Monza, Italy).

2.2. Synthesis

2.2.1. General information

All the reactions were monitored by Thin Layer chromatography (TLC) on Merck 60 F254 (0.25 mm) plates, which were visualised by UV inspection (254 nm) and/or by spraying $KMnO_4$ (0.5 g in 100 mL 0.1 N NaOH). Na_2SO_4 was used as drying agent for the organic phases. Flash chromatography purifications were performed using silica gel Merck with 60 mesh particles. Unless otherwise specified, all reagents were used as received without further purification. Dichloromethane was dried over P_2O_5 and freshly distilled under nitrogen prior to use. DMF was stored over 3 Å molecular sieves. Anhydrous THF was freshly distilled under nitrogen from Na/benzophenone ketyl. ^1H and ^{13}C NMR spectra were registered on JEOL ECZR600 spectrometer, at 600 and 151 MHz. Coupling constants (J) are given in Hertz (Hz) and chemical shifts (δ) are given in ppm, calibrated to solvent signal as internal standard. Following abbreviations are used to describe multiplicities: s = singlet, d = doublet, t = triplet, q = quadruplet, m = multiplet and br = broad signal. The following abbreviations are used to identify exact proton: ArH = Aromatic proton, BzImH = benzimidazolone ring, Pip = piperidine. ESI-mass spectra were recorded on a Waters Micromass Quattro Micro equipped with an ESI source. The purity of the final compounds was determined by RP-HPLC. Analyses were performed with a HP1100 chromatograph system (Agilent Technologies, Palo Alto, CA, USA) equipped with a quaternary pump (G1311A), a membrane degasser (G1379A) and a diode-array detector (DAD) (G1315B) integrated into the HP1100 system. Data analyses were processed using a HP ChemStation system (Agilent Technologies). The analytical column was a LiChrospher 100 C18-e (250 × 4.6 mm, 5 μm) (Merck KGaA, 64271 Darmstadt, Germany) eluted with CH_3CN 0.1 % TFA/H_2O 0.1 % TFA in a ratio that depended on the characteristics of the compound. All compounds were dissolved in the mobile phase at a concentration of about 0.01 mg/mL and injected through a 20 μl loop. HPLC retention times (tR) were obtained at flow rates of 1.0 mL/min and the column effluent was monitored by DAD at 226 and 254 nm (with 800 nm as the reference wavelength). The purity of the samples was evaluated as the percentage ratio between the areas of the main peak and of possible impurities at the two wavelengths, and also using a DAD purity analysis of the chromatographic peak. The purity of all the target compounds was found to be greater than 95 %. Compounds **1** [19], **2**–**4** [25] were synthesized according to the reported procedures.

2.2.2. (2,6-Dichlorobenzoyl)-L-asparagine (5)

2,6-Dichlorobenzoic acid (0.500 g; 5.13 mmol) was dissolved in $SOCl_2$ (10 mL; 5.1 mmol) and heated at 70 °C for 18 h. Excess $SOCl_2$ was evaporated under reduced pressure and the residual acyl chloride was co-evaporated with THF (3 × 30 mL). The resulting yellowish oil was dissolved in 1,4-dioxane (10 mL) and added dropwise to a solution of L-asparagine (0.343 g; 2.59 mmol) and Na_2CO_3 (0.806 g; 6.50 mmol) in H_2O (10 mL). The reaction mixture was stirred at rt for 18 h, treated with HCl (1.0 M, 20 mL) and extracted with EtOAc (3 × 30 mL). The combined organic fractions were washed with brine (30 mL), dried and concentrated under reduced pressure. The residue was purified by flash column chromatography eluting with DCM to DCM/MeOH 95:5. The fractions containing the desired product were concentrated under reduced pressure affording 0.359 g (45 %) of **5** as a white solid. ^1H NMR (600 MHz, DMSO-d_6) δ = 12.62 (br s, 1H, COOH), 8.92 (d, J = 7.9 Hz, 1H, NH), 7.47-(two overlapping doublets, J = 8.95 and J = 7.23 Hz, 2H), 7.41 (dd, J = 8.95, 7.06 Hz, 1H), 7.37 (br s, 1H, $CONH_A$), 6.92 (br s, 1H, $CONH_B$), 4.71 (ABMX system, complex m, 1H, CH), 2.69 (dd, J = 15.7, 6.89 Hz, 1H, CH_A), 2.49 (dd, partially overlapping with solvent signal, J = 15.7, 6.37 Hz, 1H, CH_B). ^{13}C NMR (151 MHz, DMSO-d_6) δ = 172.6, 171.5, 163.6, 136.6, 131.8, 131.5, 128.5, 49.6, 37.2. MS (ESI$^-$): m/z 303/305/307 $[M-H]^-$.

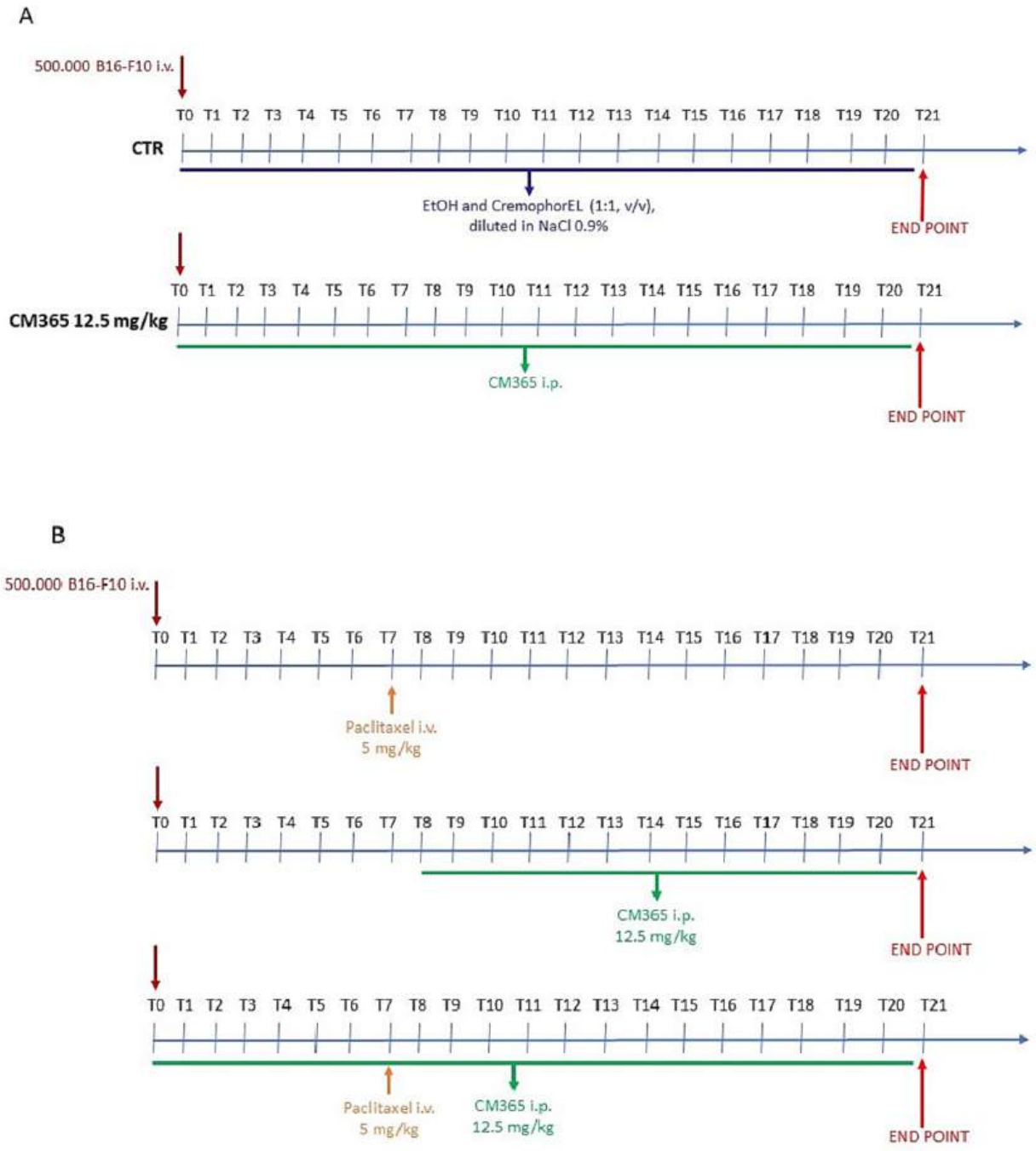

Fig. 2. Experimental protocols of lung metastasis mouse model of melanoma.

*2.2.3. (R)-(2,6-Dichlorobenzoyl)aspartic acid (**6**)*

The reaction was run with 2,6-dichlorobenzoic acid (0.33 g, 1.77 mmol), $SOCl_2$ (2 mL), di-*tert*-butyl D-aspartate (0.50 g, 1.77 mmol), K_2CO_3 (0.49 g, 3.5 mmol) in THF (10 mL). The crude product was purified by flash chromatography (DCM to DCM/MeOH 95:5) to give the protected acid (2.22 g, 99.8 %) as a colourless oil. The protected acid (0.680 g, 1.63 mmol) was dissolved in TFA 10 % in DCM (20 mL) and stirred at rt overnight. The mixture was diluted with DCM and washed with 0.1 M HCl solution (3 × 25 mL) and brine (10 mL). The organic phases were dried and concentrated under reduced pressure. The obtained product was purified by flash chromatography (DCM/MeOH 95:5) to give **6** (0.301 g, 55 % from starting acid) as a white solid. ^{1}H NMR (600 MHz, DMSO-d_6) $\delta = 12.65$ (br s, 2H), 9.05 (d, $J = 7.9$ Hz, 1H), 7.48 (two overlapping doublets, J = 9.0 and $J = 7.1$ Hz, 2H), 7.38 (dd, $J = 9.0$, 7.1 Hz, 1H), 4.68 (ABMX system, comple m, 1H), 2.80 (dd, $J = 16.6$, 6.4 Hz, 1H), 2.63 (dd, $J = 16.6$, 6.9 Hz, 1H). ^{13}C NMR (151 MHz, DMSO-d_6) $\delta = 172.3$, 172.0, 163.7, 136.6, 131.8, 131.6, 128.5, 49.4, 36.5. MS (ESI$^-$): *m/z* 304/306/308 $[M-H]^-$.

*2.2.4. General procedure for the preparation of compounds **7–9***

A solution of 2,6-dichlorobenzoic acid (0.333 g, 1.75 mmol) in $SOCl_2$ (5 mL) was heated under reflux for 1 h. Volatiles were evaporated under reduced pressure and the residue was added to a stirred solution of the appropriate aminoacid esters (1.1 mmol) in THF (5 mL) and triethylamine (4.36 mmol) and stirred at room temperature for 3 h. The solvent was evaporated under reduced pressure and the residue taken-up with a saturated solution of NH_4Cl (50 mL) and extracted with EtOAc (3 × 25 mL). The combined organic phases were washed with brine (25 mL),

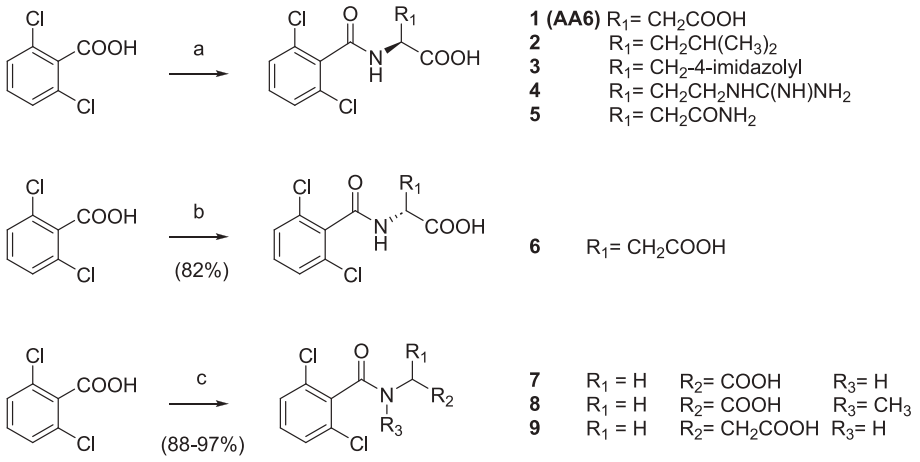

Scheme 2. Reagents and conditions: (a) (i) $SOCl_2$, 70 °C, 18 h; (ii) 1,4-dioxane, appropriate amine, Na_2CO_3 /H_2O, rt, 18 h. (b) (i) $SOCl_2$, 70 °C, 2 h, D-aspartic acid *tert*-butyl ester (1.1 eq), DIPEA (3 eq), DMF, rt, 18 h; (ii) TFA/DCM (10 %), rt, 18 h. (c) (i) $SOCl_2$, 70 °C, 18 h; (ii) 1,4-dioxane, appropriate amine, Et_3N (3 eq), DMF, rt, 18 h; (iii) LiOH 2 N, EtOH, rt, 18 h.

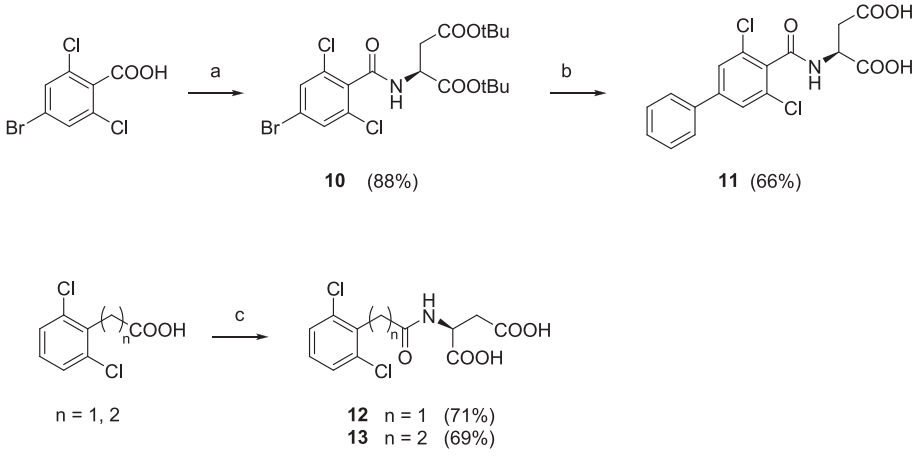

Scheme 3. Reagents and conditions: (a) $SOCl_2$, 80 °C, 2 h; L-aspartic acid *tert*-butyl ester (1.1 eq), DIPEA (3 eq), DMF, rt, 18 h. (b) (i) phenylboronic acid (1 eq), Pd $(PPh_3)_4$ (5 %mol), K_2CO_3 (2 eq), 1,4-dioxane/water (4:1), 90 °C, 3 h; (ii) TFA/DCM (10 %), rt, 18 h. (c) (i) DIPEA (3.0 eq), HBTU (1.5 eq), HOBT (0.10 eq), L-aspartic acid *tert*-butyl ester (1.1 eq), DMF, rt, 18 h; (ii) TFA/DCM (10 %), rt, 18 h.

dried and concentrated under reduced pressure. The obtained ethyl ester was not further purified and was treated with a solution of LiOH 2 M (10 M equivalents) and THF (5 mL) and stirred at rt for 18 h. The mixture was acidified with 1 M HCl (10 mL) and extracted with DCM (3 × 25 mL), dried and concentrated under reduced pressure to afford the desired compounds.

2.2.5. (2,6-Dichlorobenzoyl)glycine (7)

The reaction was run with ethyl glycinate hydrochloride (0.269 g, 1.93 mmol) as the amine using the above reported procedure to obtain **7** (0.416 g, 96 %) was isolated as a white solid. ^{1}H NMR (600 MHz, DMSO-D6) $\delta = 12.6$ (br s, 1H), 9.02 (t, $J = 5.7$ Hz, 1H), 7.45 (two overlapping doublets, J = 8.95 and $J = 7.06$ Hz, 2H), 7.39 (dd, $J = 8.95$, 7.06 Hz, 1H), 3.94 (d, $J = 5.7$ Hz, 2H). ^{13}C NMR (151 MHz, DMSO-D6) $\delta = 171$, 164.4, 136.7, 131.8, 131.6, 128.6, 41.3. MS (ESI$^-$): *m/z* 246/248/250 $[M-H]^-$.

2.2.6. N-(2,6-Dichlorobenzoyl)-N-methylglycine (8)

The reaction was run with sarcosine ethyl ester hydrochloride (0.296 g, 1.93 mmol) as the amine using the above reported procedure to obtain **8** (0.404 g, 88 %) as a white solid. In NMR spectra recorded at 20 °C in DMSO-D6 the presence of two rotamers present in approx. 78:22 % ratio is evidenced. ^{1}H NMR (600 MHz, DMSO-D6) $\delta = 12.8$ (br s, 1H), 7.56 (two doublets, $J = 8.8$, 7.6 Hz, 2H, rotamer A), 7.54 (two doublets, $J = 8.8$, 7.4 Hz, 2H, rotamer B), 7.48–7.44 (two overlapped dd, given by rotamers A + B, 1H), 4.22 (s, 2H, rotamer A), 3.86 (s, 2H, rotamer B), 3.08 (s, 3H, rotamer B), 2.83 (s, 3H, rotamer A). ^{13}C NMR (151 MHz, $CDCl_3$). Rotamer A: $\delta = 170.3$, 165.2, 135.2, 131.1, 128.96, 48.3, 36.5. Rotamer B: $\delta = 170.1$, 164.9, 134.8, 131.4, 129.04, 51.4, 33.8. MS (ESI$^-$): *m/z* 260/262/264 $[M-H]^-$.

2.2.7. 3-(2,6-Dichlorobenzamido)propanoic acid (9)

The reaction was run with β-alanine ethyl ester hydrochloride (0.296 g, 1.93 mmol) as the amine using the above reported procedure to obtain **9** (0.445 g, 97 %) as a white solid. ^{1}H NMR (600 MHz, DMSO-D6) $\delta = 12.3$ (br s, 1H), 8.76 (t, $J = 5.5$ Hz, 1H), 7.48 (two overlapping doublets, J = 8.9 and $J = 7.2$ Hz, 2H), 7.41 (dd, $J = 8.9$, 7.2 Hz, 1H), 3.45–3.40 (ABMX system, m, 2H), 2.50–2.49 (ABMX system, m, partially overlapping with solvent signal, 2H). ^{13}C NMR (151 MHz, $CDCl_3$) $\delta = 175.0$, 165.0, 164.9, 135.8, 132.2, 130.7, 128.1, 35.4, 35.2, 33.5. MS (ESI$^-$): *m/z* 260/262/264 $[M-H]^-$.

2.2.8. Di-tert-butyl (4-bromo-2,6-dichlorobenzoyl)-L-aspartate (10)

4-Bromo-2,6-dichlorobenzoic acid (0.400 g, 1.48 mmol) was

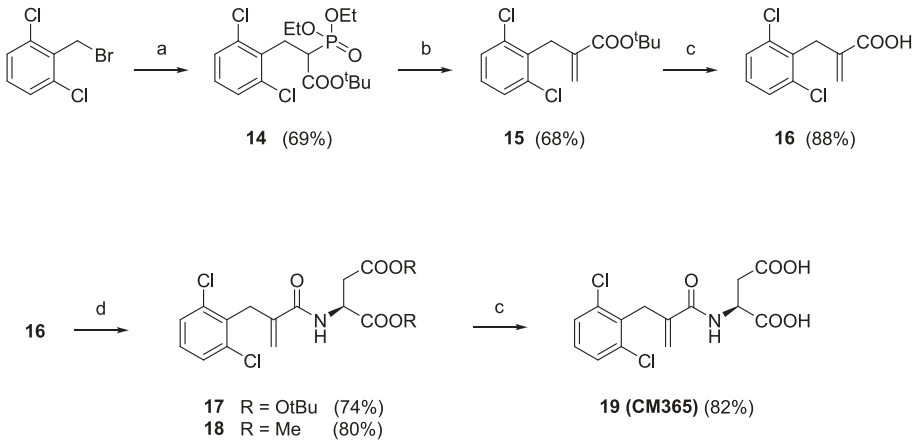

Scheme 4. Reagents and conditions: (a) *tert*-butyl diethylphosphonoacetate (1.2 eq), NaH (1.4 eq), DMF, rt, 2 h. (b) paraformaldehyde (8 eq), K_2CO_3 (3 eq), water, 90 °C, 72 h. (c) TFA/DCM (10 %), rt, 18 h. (d) L-aspartic acid di-*tert*-butyl ester (1.1 eq) or L-aspartic acid dimethyl ester, HBTU (1.5 eq), HOBt (0.1 eq), DIPEA (3 eq), DMF, 18 h.

dissolved in $SOCl_2$ (4 mL) and heated under reflux for 1 h. The volatiles were evaporated under reduced pressure, and the residue was dissolved in dry THF (5 mL). The solution was added in a stirred solution of di-*tert*-butyl L-aspartate (0.417 g, 1.48 mmol) and K_2CO_3 (0.410 g, 2.96 mmol) in THF (10 mL). The mixture was stirred at rt for 3 h. The solvent was evaporated under reduced pressure. The residue was dissolved in EtOAc (25 mL) and a saturated solution of NH_4Cl (25 mL) was added. The compound was extracted with EtOAc (3 × 50 mL). The combined organic phases were washed with brine (150 mL), dried and concentrated under reduced pressure. The crude product was purified by flash

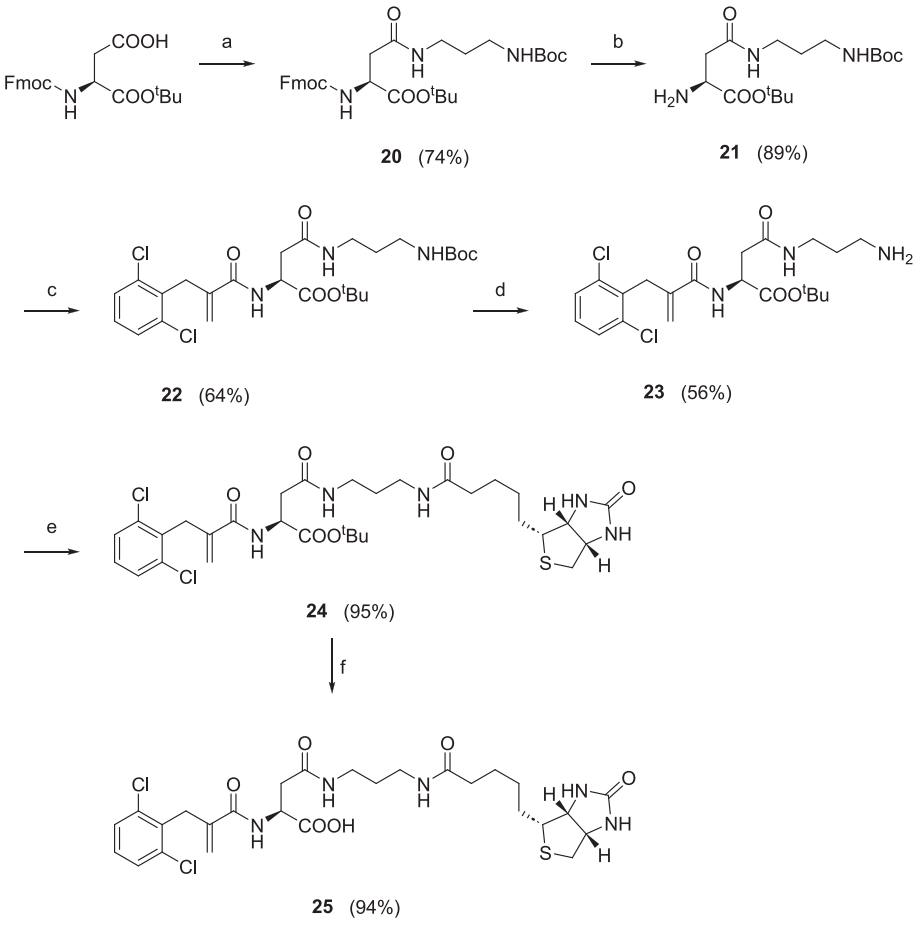

Scheme 5. Reagents and conditions: (a) *N*-boc diaminopropane (1.2 eq), CDI (1.1 eq), THF, rt, 7 h. (b) piperidine (5 eq), DMF, rt, 3 h. (c) (i) **16** (1 eq), oxalyl chloride (1.1 eq), DCM, 0 °C, 1 h; (ii) DIPEA (2.5 eq), **21** (1.1 eq), DCM, rt, 3 h. (d) TFA (3 eq) in DCM, 0 °C to rt, 48 h. (e) Biotin-NHS ester (1 eq), DIPEA (1 eq), DMF, rt, 18 h. (f) TFA/DCM (10 %), rt, 18 h.

Table 1
Inhibition of B16-F10 cells invasion.

Compound	Maximal efficacy [a] % inhibition at 100 μM ± SE	IC_{50} (μM) ± SE [b]
1 AA6	70 ± 4	0.7 ± 0.1
2	29 ± 2	nc [c]
3	42 ± 1	nc [c]
4	52 ± 2	45 ± 9
5	65 ± 5	0.7 ± 0.4
6	not active	nc [c]
7	45 ± 3	nc [c]
8	39 ± 2	nc [c]
9	41 ± 1	nc [c]
11	35 ± 2	nc [c]
12	55 ± 5	4.5 ± 3
13	60 ± 4	2.4 ± 1
18	not active	nc [c]
19 CM365	60 ± 3	5.5 ± 3.8
25	56 ± 7	0.46 ± 0.18

[a] Percentage inhibition of B16-F10 cells invasiveness at the maximal concentration tested (100 μM) versus control invasion measured on untreated cells.
[b] IC_{50} values calculated for the most active compounds (maximal efficacy at 100 μM > 50 %).
[c] not calculated.

chromatography (PE /EtOAc 95:5 to 9:1) to give **10** (0.650, 88 %) as a colourless oil. ^{1}H NMR (600 MHz, $CDCl_3$) δ = 7.48 (s, 2H), 6.87 (d, J = 7.9 Hz, 1H), 4.82–4.80 (ABMX system, m, 1H), 3.00 (dd, J = 17.6, 4.2 Hz, 1H), 2.94 (dd, J = 17.6, 4.1 Hz, 1H), 1.45 (s, 9H), 1.41 (s, 9H). ^{13}C NMR (151 MHz, $CDCl_3$) δ = 170.4, 169.1, 163.0, 134.6, 133.1, 130.9, 123.4, 82.8, 81.7, 49.6, 37.0, 28.1, 28.0. MS (ESI^+): *m/z* 496/498/500 $[M + H]^+$.

2.2.9. *(3,5-Dichloro-[1,1′-biphenyl]-4-carbonyl)-L-aspartic acid* (**11**)

To a stirred solution of **10** (0.150 g, 0.302 mmol) in dioxane/water (6 mL/1.5 mL), phenyl boronic acid (0.037 g, 0.302 mmol), $Pd(PPh_3)_4$ (0.017 g, 0.015 mmol) and K_2CO_3 (0.084 g, 0.604 mmol) were added. The mixture was stirred at 80 °C for 3 h. The solvent was evaporated under reduced pressure and the obtained residue dissolved in DCM (15 mL) and water (15 mL). The compound was extracted with DCM (3 × 15 mL). The combined organic phases were washed with brine (15 mL), dried and concentrated under reduced pressure. The crude product was purified by flash chromatography (PE /EtOAc 95:5 to 9:1) to give di-*tert*-butyl (3,5-dichloro-[1,1′-biphenyl]-4-carbonyl)-L-aspartate (0.100, 67.1 %) as a colourless oil. MS (ESI^+): *m/z* 494/496/498 $[M + H]^+$.The protected intermediate (0.090 g, 0.182 mmol) was dissolved in a stirred solution of TFA/DCM (10 %, 3 mL) at rt. After 18 h the mixture was concentrated under reduced pressure. The crude product was purified by flash chromatography (DCM/MeOH 95:5) to give **11** (0.067 g, 58 % from **10**) as a white solid. ^{1}H NMR (600 MHz, DMSO-d_6) δ = 12.65 (s, br, 2H), 9.14 (d, J = 8.1 Hz, 1H), 7.79–7.75 (two overlapping signals, m, 4H), 7.50 (t, J = 7.4 Hz, 2H), 7.45 (t, J = 7.4 Hz, 1H), 4.76 (ABMX system, m, 1H), 2.82 (dd, J = 16.5, 6.2 Hz, 1H), 2,65 (dd, J = 16.5, 7.1 Hz, 1H). ^{13}C NMR (151 MHz, DMSO-d_6) δ = 172.2, 172, 163.7, 143.4, 137.4, 135.2, 132.4, 129.7, 129.4, 127.6, 126.4, 49.5, 36.4. MS (ESI^-): *m/z* 380/382/384 $[M-H]^-$.

2.2.10. *(2-(2,6-Dichlorophenyl)acetyl)-L-aspartic acid* (**12**)

2,6-Dichlorophenylacetic acid (0.250 g, 1.22 mmol) was dissolved in a stirred solution of di-*tert*-butyl L-aspartate (0.378 g, 1.34 mmol), DIPEA (0.608 mL, 3.66 mmol), HOBt (0,016 g, 0,120 mmol), and HBTU (0.694 g, 1.83 mmol) in DMF (3 mL) at room temperature and the mixture was stirred overnight. The solvent was evaporated under reduced pressure and a solution of $NaHCO_3$ 10 % (15 mL) was added. The mixture was extracted with EtOAc (3 × 10 mL). The combined organic phases were washed with brine (15 mL), dried, and concentrated under reduced pressure. The crude product was purified by flash chromatography (PE/EtOAc 9:1) to give the protected intermediate (0.505 g, 95 %). The protected intermediate (0.500 g; 1.15 mmol) was dissolved in TFA/DCM (10 %, 15 mL) and stirred overnight at RT. After evaporation of the solvent, the product was purified by flash chromatography (DCM/MeOH 95:5) to give **12** (0.260 g, 67 % from starting acid) as a white solid. ^{1}H NMR (600 MHz, DMSO-D6) δ = 12.57 (br s, 2H), 8.47 (d, J = 7.9 Hz, 1H), 7.43 (d, J = 8.4 Hz, 2H), 7.30 (t, J = 8.4 Hz, 1H), 4.52 (ABMX

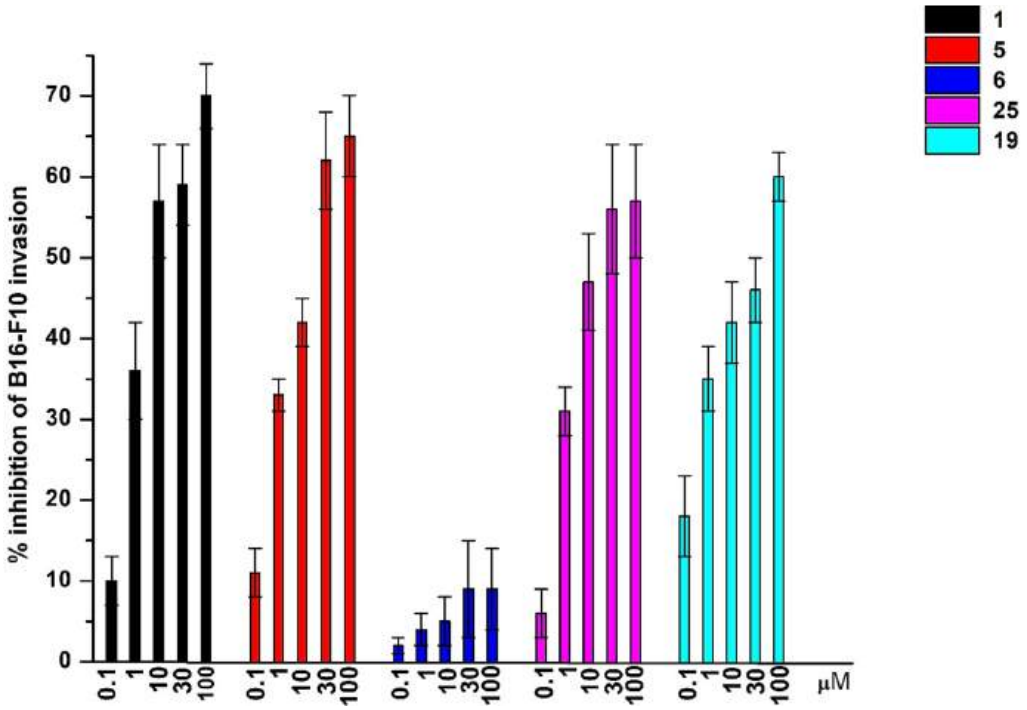

Fig. 3. Concentration-response curves for invasion assay in B16-F10 cells treated with different compounds (0.1–100 μM). Data are expressed as percentages of inhibition of cell invasion versus the control invasion measured on untreated cells. The data are shown as the mean ± SEM of 5 independent experiments.

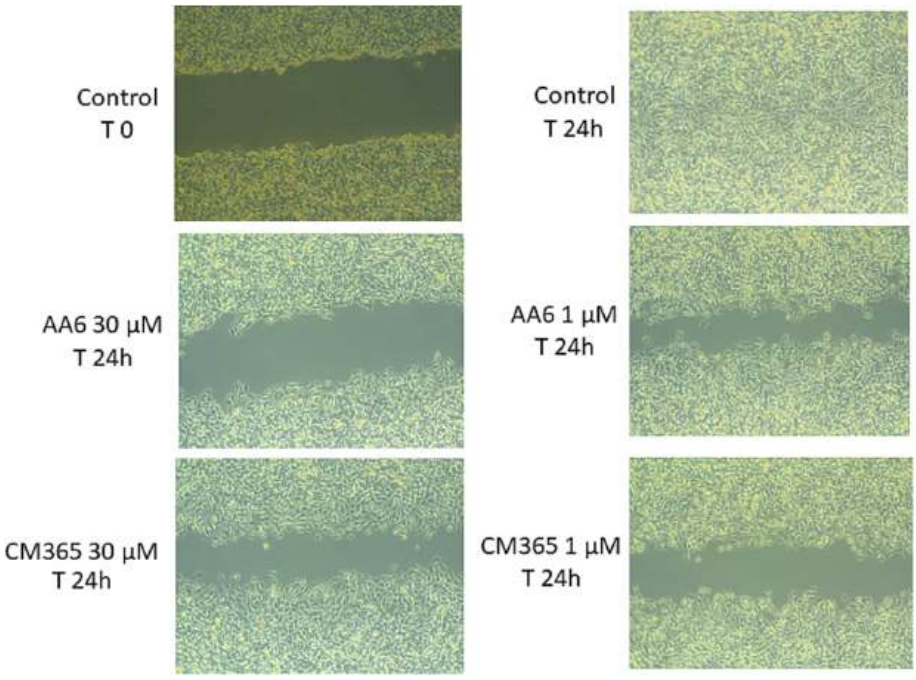

Fig. 4. Wound healing assay at 0 (T0) and at 24 h in B16-F10 cells untreated (Control) or treated with AA6 or CM365 (1 and 30 μM). Original magnification 10x; panels show a representative experiment (n = 3).

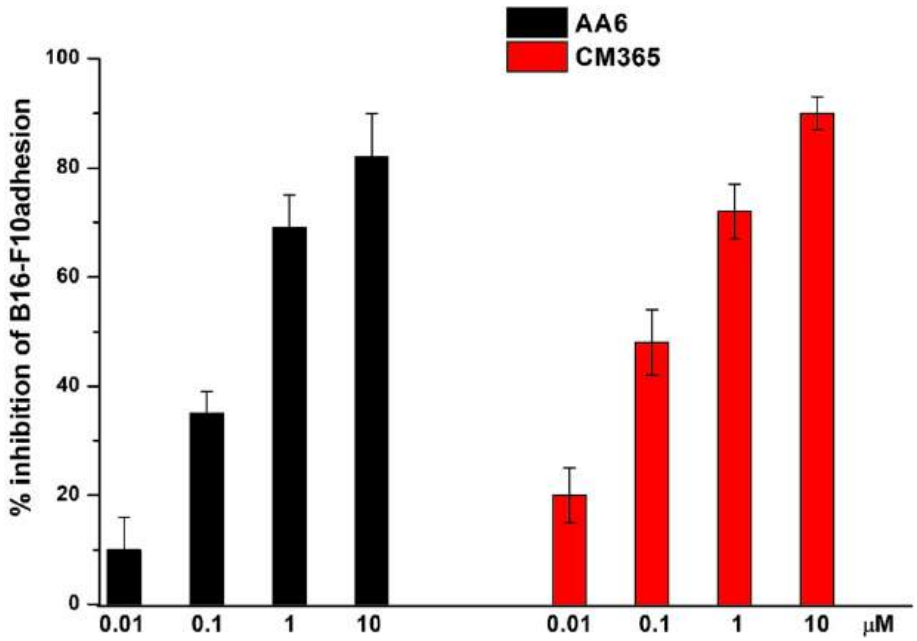

Fig. 5. Inhibition of B16-F10 cells adhesion to MS1 cells. MS1 were pre-treated with increasing concentrations of compounds AA6 and CM365 (0.01–10 μM) for 18 h and then incubated with B16-F10 for 45 min. Data are expressed as mean ± SEM (n = 5) of the percentage of inhibition versus control adhesion detected on untreated MS1.

system, complex m, 1H), 3.83 (s, 2H), 2.68 (dd, J = 16.2, 6.6 Hz, 1H), 2.58 (dd, J = 16.8, 6.6 Hz, 1H). ^{13}C NMR (151 MHz, DMSO-d_6) δ = 172.8, 172.2, 168.0, 136.1, 132.9, 129.8, 128.6, 49.3, 37.8, 36.6. MS (ESI$^-$): m/z 318/320/322 [M−H]$^-$.

*2.2.11. (3-(2,6-Dichlorophenyl)propanoyl)-L-aspartic acid (**13**)*

3-(2,6-Dichlorophenyl)propionic acid (0.500 g, 2.28 mmol) was dissolved in a stirred solution of di-*tert*-butyl L-aspartate (0.707 g, 2.51 mmol), DIPEA (1.17 mL, 6.85 mmol), HOBt (0.016 g, 0.120 mmol), and HBTU (1.30 g, 3.42 mmol) in DMF (3 mL) at rt and the mixture was stirred overnight. The solvent was evaporated under reduced pressure and a solution of $NaHCO_3$ 10 % (15 mL) was added. The mixture was extracted with EtOAc (3 × 10 mL). The combined organic phases were washed with brine (15 mL), dried, and concentrated under reduced pressure. The crude product was purified by flash chromatography (PE/EtOAc 9:1) to give the protected intermediate (0.914 g, 90 %). The

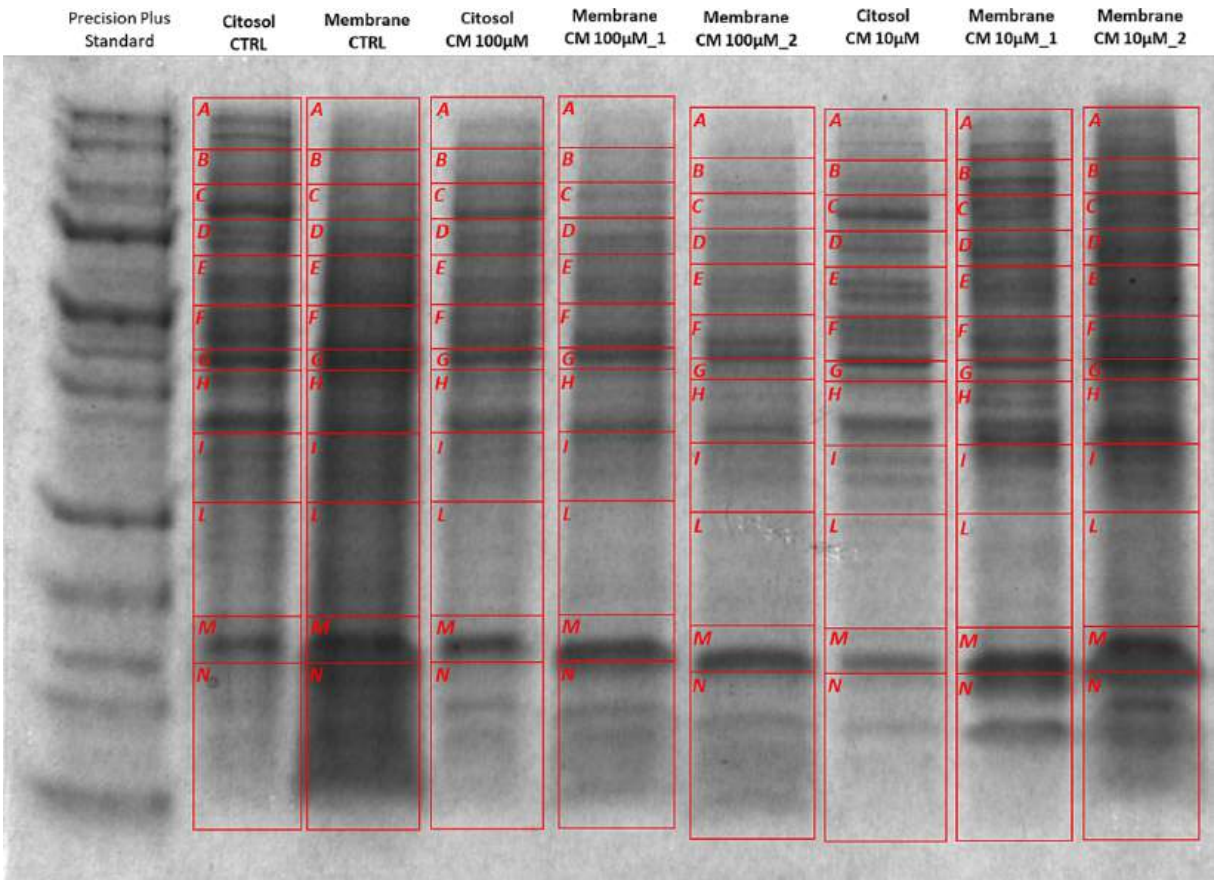

Fig. 6. SDS-PAGE of protein extracts. Precision Plus Standard: molecular mass ladder. Samples: lane 2. Untreated cytosolic protein fraction; lane 3. Untreated membrane protein fraction; lane 4. 100 µM CM365 treated cytosolic protein fraction; lane 5. 100 µM CM365 treated membrane protein fraction, replicate 1; lane 6. 100 µM CM365 treated membrane protein fraction, replicate 2; lane 7. 10 µM CM365 treated cytosolic protein fraction; lane 8. 10 µM CM365 treated membrane protein fraction, replicate 1; lane 9. 10 µM CM365 treated membrane protein fraction, replicate 2. Staining with colloidal Coomassie blue.

Table 2
Data table summarizing results report organized by protein groups, peptide groups and peptide spectral matches (PSMs).

Fraction	Protein Groups[1]	Peptide Groups[2]	PSMs[3]
M_CT (*11 bands*)	1288	4778	27,879
M_CM365_10µM (*11 bands*)	1699	6035	25,622
M_CM365_100µM (*11 bands*)	809	2730	13,153

[1] Protein Groups displays the total number of protein groups a particular protein belongs to.
[2] Peptides Groups displays the total number of distinct peptide sequences identified.
[3] PSMs displays the number of identified peptide spectrum matches. This is an indicator of the protein abundance.

protected intermediate (0.780 g, 1.75 mmol) was dissolved in TFA/DCM (10 %, 20 mL) and the mixture stirred overnight at rt. After evaporation of the solvent, the product was purified by flash chromatography (DCM/MeOH 95:5) to give **13** (0.400 g, 53 % from starting acid) as a white solid. ^{1}H NMR (600 MHz, DMSO-D6) $\delta = 12.6$ (br s, 1H), 8.30 (d, $J = 8.1$ Hz, 1H), 7.45 (d, $J = 8.1$ Hz, 2H), 7.27 (t, $J = 8.1$ Hz, 1H), 4.55 (ABMX system, complex m, 1H), 3.08–3.05 (ABMX system, complex m, 2H), 2.70 (dd, $J = 16.5$, 5.9 Hz, 1H), 2.60 (dd, $J = 16.5$, 7.2 Hz, 1H), 2.35–2.32 (ABMX system, complex m, 2H). ^{13}C NMR (151 MHz, DMSO-D6) $\delta = 174.8$, 174.6, 174.0, 137.7, 136.4, 129.6, 129.5, 50.7, 37.5, 34.8, 28.2. MS (ESI$^-$): *m/z* 332/334/336 $[M-H]^-$.

2.2.12. *tert-Butyl 3-(2,6-dichlorophenyl)-2-(diethoxyphosphoryl) propanoate (**14**)*

The reaction was conducted adapting the previously published procedure [26]. To a stirred solution of *tert*-butyl diethylphosphonoacetate (0.466 mL, 1.98 mmol) in DMF (4 mL) kept under nitrogen at 0 °C, NaH 60 % in mineral oil (0.093 g, 2.31 mmol) was added. The reaction mixture was stirred for 2 h at rt. Then, 2,6-dichlorobenzylbromide (0.396 g, 1.65 mmol) was added dropwise at 0 °C and the solution was stirred for 2 h at rt. The reaction mixture was cooled to 0 °C and water was added (40 mL). The product was extracted with DCM (3 × 50 mL), the organic layers were dried, and concentrated under reduced pressure. The crude product was purified by flash chromatography (PE/EtOAc 9:1 to 7:3) to give **14** (0.590 g, 87 %) as a colourless oil which was used directly in the next step.

2.2.13. *tert-Butyl 2-(2,6-dichlorobenzyl)acrylate (**15**)*

To a stirred solution of **14** (4.00 g, 9.72 mmol) and paraformaldehyde (2.9 g, 97.2 mmol) in water (70 mL), a solution of K_2CO_3 (6.71 g, 48.6 mmol) in water (10 mL) was added and the reaction mixture was heated under reflux for 2 days. The mixture was cooled to rt and extracted with EtOAc (3 × 40 mL). The combined organic phases were washed with brine (15 mL), dried, and concentrated under reduced pressure. The crude product was purified by flash chromatography (PE/EtOAc 95:5) to give **15** (2.7 g, 60 %) as a colourless oil. ^{1}H NMR (600 MHz, $CDCl_3$) $\delta = 7.28$ (d, $J = 8.3$ Hz, 2H), 7.10 (t, $J = 7.9$ Hz, 1H), 6.06 (s, 1H), 4.86 (s, 1H), 3.88 (s, 2H), 1.51 (s, 9H). ^{13}C NMR (151 MHz, $CDCl_3$) $\delta = 165.9$, 137.9, 136.2, 135.3, 128.4, 128.2, 123.4, 81.0, 32.9, 28.2.

A.

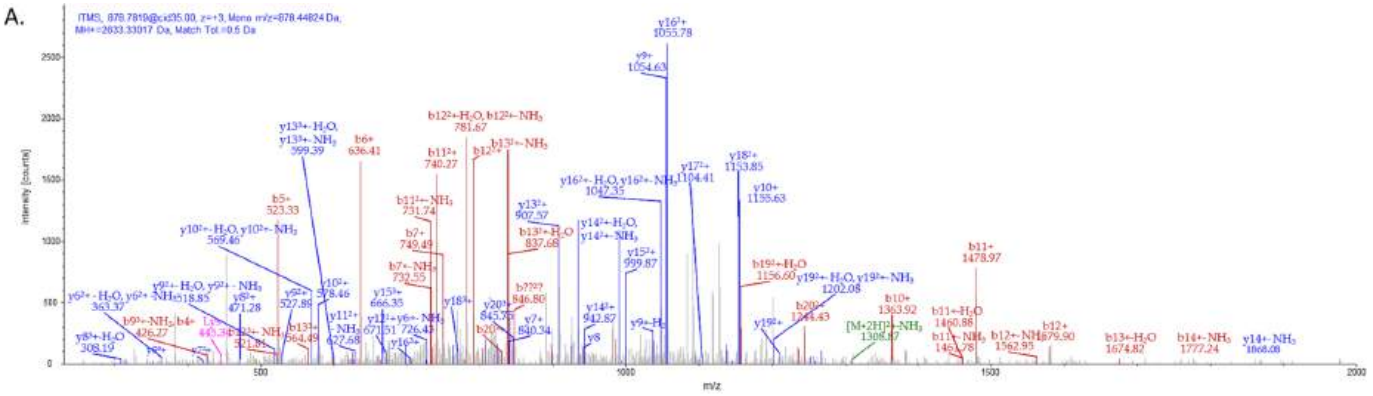

B.

#1	Immonium	b¹⁺	b²⁺	b³⁺	Seq.	y¹⁺	y²⁺	y³⁺	#2
1	72.08078	100.07569	50.54148	34.03008	V				21
2	87.05529	214.11862	107.56295	72.04439	N	2534.25849	1267.63289	845.42435	20
3	86.09643	327.20268	164.10498	109.73908	I	2420.21557	1210.61142	807.41004	19
4	72.08078	426.27110	213.63919	142.76188	V	2307.13150	1154.06939	769.71535	18
5	70.06513	523.32386	262.16557	175.11280	P	2208.06309	1104.53518	736.69255	17
6	86.09643	636.40792	318.70760	212.80749	I	2111.01032	1056.00880	704.34163	16
7	86.09643	749.49199	375.24963	250.50218	L	1997.92626	999.46677	666.64694	15
8	44.04948	820.52910	410.76819	274.18122	A	1884.84220	942.92474	628.95225	14
9	445.11658	1292.63331	646.82030	431.54929	K-CM365	1813.80508	907.40618	605.27321	13
10	44.04948	1363.67043	682.33885	455.22833	A	1341.70087	671.35407	447.90514	12
11	88.03930	1478.69737	739.85232	493.57064	D	1270.66376	635.83552	424.22610	11
12	74.06004	1579.74505	790.37616	527.25320	T	1155.63681	578.32205	385.88379	10
13	86.09643	1692.82911	846.91819	564.94789	L	1054.58914	527.79821	352.20123	9
14	74.06004	1793.87679	897.44203	598.63045	T	941.50507	471.25617	314.50654	8
15	70.06513	1890.92956	945.96842	630.98137	P	840.45739	420.73233	280.82398	7
16	70.06513	1987.98232	994.49480	663.33229	P	743.40463	372.20595	248.47306	6
17	102.05496	2117.02491	1059.01609	706.34649	E	646.35187	323.67957	216.12214	5
18	72.08078	2216.09333	1108.55030	739.36929	V	517.30927	259.15827	173.10794	4
19	88.03930	2331.12027	1166.06377	777.71161	D	418.24086	209.62407	140.08514	3
20	129.11347	2487.22138	1244.11433	829.74531	R	303.21392	152.11060	101.74282	2
21	101.10732				K	147.11280	74.06004	49.70912	1

Fig. 7. A) Fragmentation spectrum of the $[M + 3H]^{3+}$ precursor ion at *m/z* 878.44824 identified by computational analysis (*modified fragment ion). B) Corresponding theoretical fragmentation pattern obtained by means of the software *Proteome Discoverer*.

*2.2.14. 2-(2,6-Dichlorobenzyl)acrylic acid (**16**)*

Compound **15** (2.7 g, 5.88 mmol) was dissolved in a stirred solution of TFA/DCM (10 %, 50 mL) at rt. After 12 h the mixture was concentrated under reduced pressure. The crude product was purified by flash chromatography (DCM/MeOH 95:5) to give **16** (1.19 g, 88 %) as a white solid. ^{1}H NMR (600 MHz, $CDCl_3$) $\delta = \delta$ 7.33 (d, $J = 8.3$ Hz, 2H), 7.16 (t, $J = 8.1$ Hz, 1H), 6.36 (s, 1H), 5.11 (s, 1H), 3.96 (s, 2H). ^{13}C NMR (151 MHz, $CDCl_3$) $\delta = 172.5, 136.3, 135.7, 134.6, 128.7, 128.4, 127.3, 32.5$.

*2.2.15. General procedure for the preparation of compounds **17** and **18***

To a stirred solution of **16** (1 eq) in DMF (2 mL), DIPEA (2.2 eq), HOBt (0.15 eq), HBTU (1.5 eq), and di-*tert*-butyl L-aspartic acid hydrochloride or dimethyl L-aspartic acid hydrochloride (1.1 eq) were added at rt and the mixture was stirred overnight. The solvent was evaporated under reduced pressure and an aqueous solution of $NaHCO_3$ 10 % (20 mL) was added. The mixture was extracted with EtOAc (3 × 20 mL). The combined organic phases were washed with brine (15 mL), dried, and concentrated under reduced pressure.

*2.2.16. Di-tert-butyl (2-(2,6-dichlorobenzyl)acryloyl)-L-aspartate (**17**)*

The reaction was conducted with **16** (0.500 g, 2.16 mmol), DIPEA (0.790 mL, 4.76 mmol), HOBt (0.041 g, 0.315 mmol), HBTU (1.19 g, 3.15 mmol), and di-*tert*-butyl L-aspartate hydrochloride (0.650 g, 2.31 mmol) in DMF (5 mL). The crude product was purified by flash chromatography (PE / EtOAc 9:1) to give **17** (0.730 g, 74 %) as a white solid. ^{1}H NMR (600 MHz, $CDCl_3$): $\delta = 7.31$ (d, J = 8.1, 2H), 7.14 (t, $J = 8.1$ Hz, 1H), 6.94 (d, $J = 7.9$ Hz, 1H), 5.66 (t, $J = 1.7$ Hz, 1H), 4.77–4.74 (two overlapping signals, m, 2H), 3.96 (m, 2H), 2.93 (dd, $J = 17$, 4.1 Hz, 1H), 2.81 (dd, $J = 17$, 4.4 Hz, 1H), 1.47 (s, 9H), 1.44 (s, 9H). ^{13}C NMR (151 MHz, $CDCl_3$) $\delta = 170.4, 170, 167.6, 140.7, 136.3, 134.8, 128.5, 128.3, 128, 118, 82.5, 81.6, 49.4, 37.6, 33.1, 28.1, 28$. MS ($ESI^+$): *m/z* 458/460/462 $[M + H]^+$.

*2.2.17. Dimethyl (2-(2,6-dichlorobenzyl)acryloyl)-L-aspartate (**18**)*

The reaction was run using **16** (0.262 g, 1.14 mmol), DIPEA (0.568 mL, 3.42 mmol), HOBt (0.015 g, 0.110 mmol), HBTU (0.648 g, 1.17 mmol), and dimethyl L-aspartate hydrochloride (0.247 g, 1.25 mmol) in DMF (4 mL). The crude product was purified by flash chromatography (PE / EtOAc 9:1) to give **18** (0.341 g, 80 %) as a white solid. ^{1}H NMR (600 MHz, DMSO-d_6) $\delta = 8.64$ (d, $J = 7.8$ Hz, 1H), 7.51 (d, $J = 8.4$ Hz, 2H), 7.35 (t, $J = 8.4$ Hz, 1H), 5.74 (t, $J = 1.8$ Hz, 1H), 4.73 (ABMX system, complex m, 1H), 4.65 (t, $J = 1.8$ Hz, 1H), 3.80 (d, $J = 1.8$ Hz, 2H), 3.64 (s, 3H), 3.62 (s, 3H), 2.90 (dd, $J = 16.2$, 6.1 Hz, 1H), 2.78 (dd, $J = 16.2$, 8.4 Hz, 1H). ^{13}C NMR (151 MHz, DMSO-d_6) $\delta = 171.4, 170.7, 167, 153.4, 139.7, 135.3, 134.5, 129.7, 128.7, 118.4, 52.4, 51.9, 49.2, 35.4, 32.9$. MS ($ESI^+$): *m/z* 374/376/378 $[M + H]^+$.

*2.2.18. (2-(2,6-Dichlorobenzyl)acryloyl)-L-aspartic acid (**19**)*

Compound **17** (0.540 g, 1.18 mmol) was dissolved in TFA/DCM 10 % (10 mL) and the reaction stirred overnight at rt. The solvent was evaporated and the crude product was recrystallised from water to give **19** (0.301 g, 74 %) as a white solid. ^{1}H NMR (600 MHz, DMSO-d_6) δ =

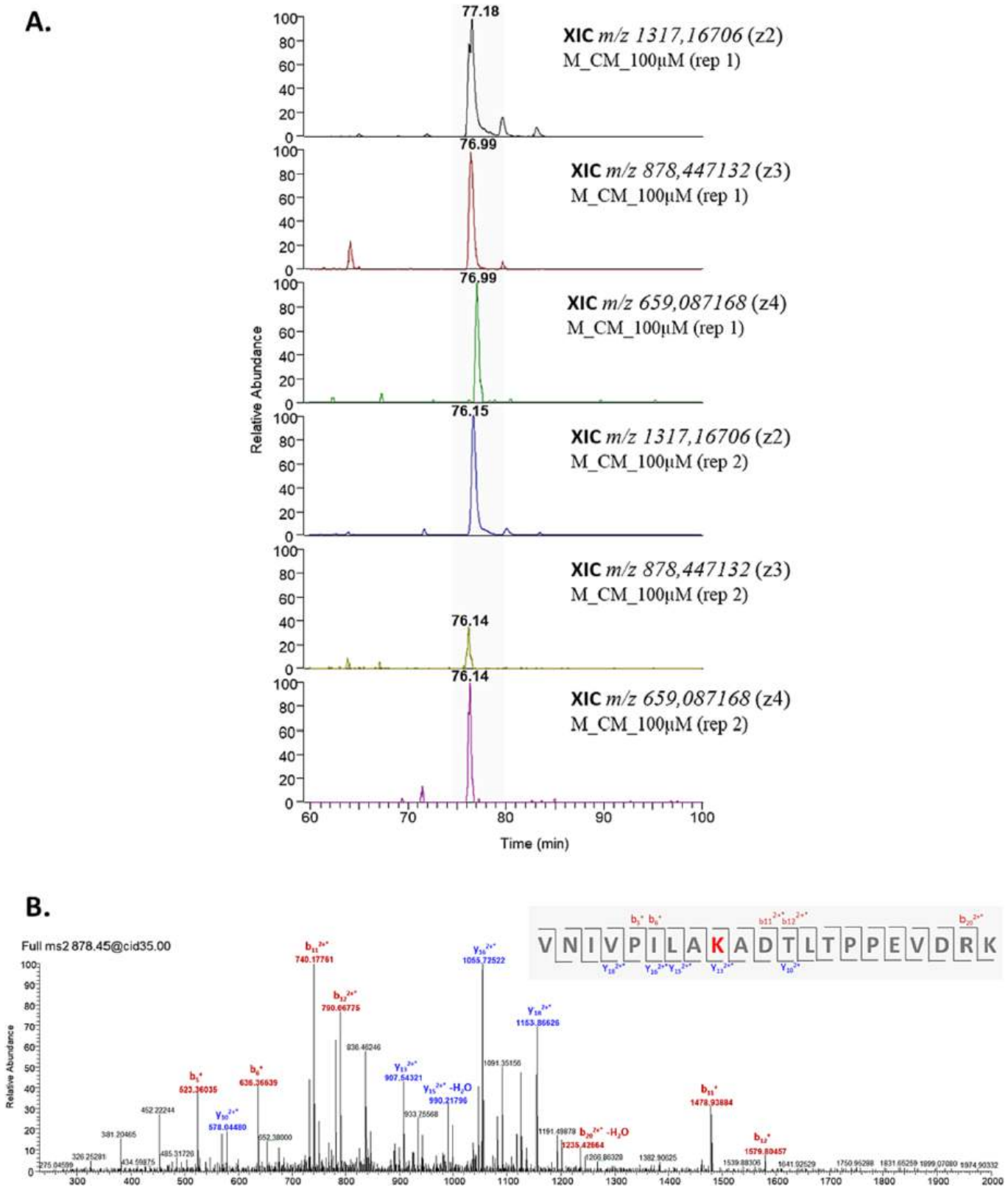

Fig. 8. A) XIC of the peptide VNIVPILAk*ADTLTPPEVDRK (*CM365-adduct) in the +2 (*m/z* 1317,16706), +3 (*m/z* 878,447132), +4 (*m/z* 659,087168) charge states, extracted in two technical replicates of M_CM_100µM. B) Manual interpretation of the experimental fragmentation pattern, attributable to the speculated sequence of the peptide bearing the CM365-adduct.

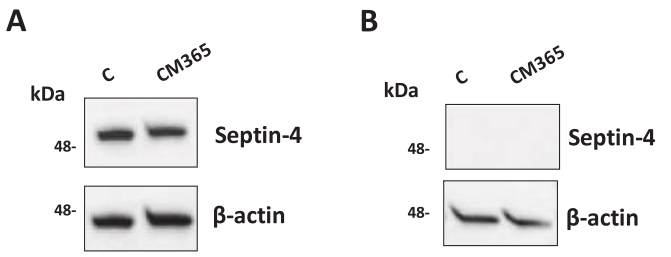

Fig. 9. Western blot analysis of septin-4 in A) B16-F10 and B) U2OS cells, untreated (C, control) or treated with CM365 (30 μM). β-actin was detected as the endogenous loading control.

12.56 (br s, 2H), 8.44 (d, $J = 7.9$ Hz, 1H), 7.51 (d, $J = 8.1$ Hz, 2H), 7.35 (t, $J = 8.1$ Hz, 1H), 5.74 (s, 1H), 4.66–4.60 (m, two overlapping signals, 2H), 3.81 (s, 2H), 2.79 (dd, $J = 16.4$, 5.8 Hz, 1H), 2.65 (dd, $J = 16.4$, 8.0 Hz, 1H). ^{13}C NMR (151 MHz, DMSO-d_6) $\delta = 173$, 172.3, 167.2, 140.2, 135.7, 134.8, 130, 129.1, 118.3, 49.6, 36.2, 33.4. MS (ESI$^-$): *m/z* 344/346/348 $[M-H]^-$.

*2.2.19. tert-Butyl N^2–(((9H-fluoren-9-yl)methoxy)carbonyl)-N^4-(3-((tert-butoxycarbonyl)amino)propyl)-L-asparaginate (**20**)*

To a stirred solution of L-Fmoc aspartate α-*tert*-butyl ester (0.979 g, 2.38 mmol) in THF (10 mL), CDI (0.425 g, 2.62 mmol) was added. After 1 h of stirring at rt, *N*-boc diaminopropane (0.500 g, 2.85 mmol) was added, and the mixture stirred for 6 h at rt. The mixture was concentrated under reduced pressure. The crude product was purified by flash chromatography (DCM/MeOH 9:1) to give **20** (1.02 g, 74 %) as a white solid. ^{1}H NMR (600 MHz, CD_3OD) $\delta = 7.77$ (d, $J = 8.1$ Hz, 2H), 7.64–7.61 (m, 2H), 7.39–7.35 (m, 2H), 7.30–7.27 (m, 2H), 4.37–4.34 (t, $J = 6.9$ Hz, 1H), 4.34–4.27 (m, 2H), 4.18 (dd, $J = 8.3$, 7.6 Hz, 1H), 3.54 (t, $J = 6.9$ Hz, 2H), 3.30–3.28 (m, 1H), 3.19–3.13 (m, 2H), 3.10–3.01 (m, 1H), 1.70 (m, 2H), 1.39 (s, 9H), 1.19 (s, 9H). ^{13}C NMR (151 MHz, CD_3OD) $\delta = 170.9$, 170.7, 157.2, 157.1, 141.2, 140.1, 128.6, 127.5, 126.9, 120.7, 82.4, 78.8, 67.7, 52.6, 47.9, 38.3, 38.1, 37.1, 30.2, 28.4, 27.9.

*2.2.20. tert-Butyl N^4-(3-((tert-butoxycarbonyl)amino)propyl)-L-asparaginate (**21**)*

To a stirred solution of **20** (0.980 g, 1.726 mmol) in DMF (5 mL), piperidine (0.852 mL, 8.631 mmol) was added and the mixture was stirred for 3 h at rt. The mixture was diluted with water (30 mL) and the product was extracted with diethyl ether (5 × 30 mL), dried, and concentrated under reduced pressure. The crude product was purified by flash chromatography (DCM/MeOH 98:2 to 9:1) to give **21** (0.530 g, 89 %) as a pale yellow oil. ^{1}H NMR (600 MHz, CD_3OD) $\delta = 3.80$ (m, 1H), 3.48 (t, $J = 6.9$ Hz, 2H), 3.18 (m, 1H), 3.04 (m, 1H), 3.00 (t, $J = 6.9$ Hz, 2H), 1.72–1.67 (q, J = 6.9, 2H), 1.41 (s, 9H), 1.19 (s, 9H). ^{13}C NMR (151 MHz, CD_3OD) $\delta = 180.1$, 176.1, 157.1, 78.7, 68.1, 51.6, 37.4, 36.3, 35.9, 29.8, 27.7, 27.4.

*2.2.21. tert-Butyl N^4-(3-((tert-butoxycarbonyl)amino)propyl)–N^2-(2-(2,6-dichlorobenzyl)acryloyl)-L-asparaginate (**22**)*

To a stirred solution of **16** (0.167 g, 0.724 mmol) in dry DCM (4 mL), oxalyl chloride (0.068 mL, 0.796 mmol) was added and the mixture was stirred for 1.5 h, at rt. The volatiles were evaporated under reduced pressure and the residue was dissolved in dry DCM (2 mL). The obtained solution was added at 0 °C in a stirred solution of **21** (0.250 g, 0.724 mmol) and DIPEA (0.308 g, 1.81 mmol) in DCM (5 mL). The mixture was stirred at rt for 3 h. The solvents were evaporated under reduced pressure. The residue was dissolved in DCM (25 mL) and water (25 mL) was added. The compound was extracted with DCM (3 × 25 mL). The combined organic phases were washed with brine (15 mL), dried, and concentrated under reduced pressure. The crude product was purified by flash chromatography (DCM/MeOH 95:5) to give **22** (0.260, 64 %) as a colourless oil. ^{1}H NMR (600 MHz, $CDCl_3$) $\delta = 7.29$ (d, $J = 8.1$ Hz, 3H), 7.12 (t, $J = 8.1$ Hz, 1H), 6.53 (br s, 1H), 4.92 (s, 1H), 4.76–4.73 (m, two overlapping signals, 2H), 3.93 (s, 2H), 3.31–3.20 (m, 2H), 3.11 (m, 2H), 2.90 (dd, $J = 15.6$, 4.2 Hz, 1H), 2.75 (dd, $J = 15.6$, 4.5 Hz, 1H), 1.57 (m, 2H), 1.45 (s, 9H), 1.40 (s, 9H). ^{13}C NMR (151 MHz, $CDCl_3$) $\delta = 170.5$, 170.1, 167.8, 156.7, 140.4, 136.3, 134.8, 128.5, 128.3, 118.3, 82.4, 79.5, 49.9, 37.7, 37.0, 36.0, 33.1, 30.3, 28.5, 28.0.

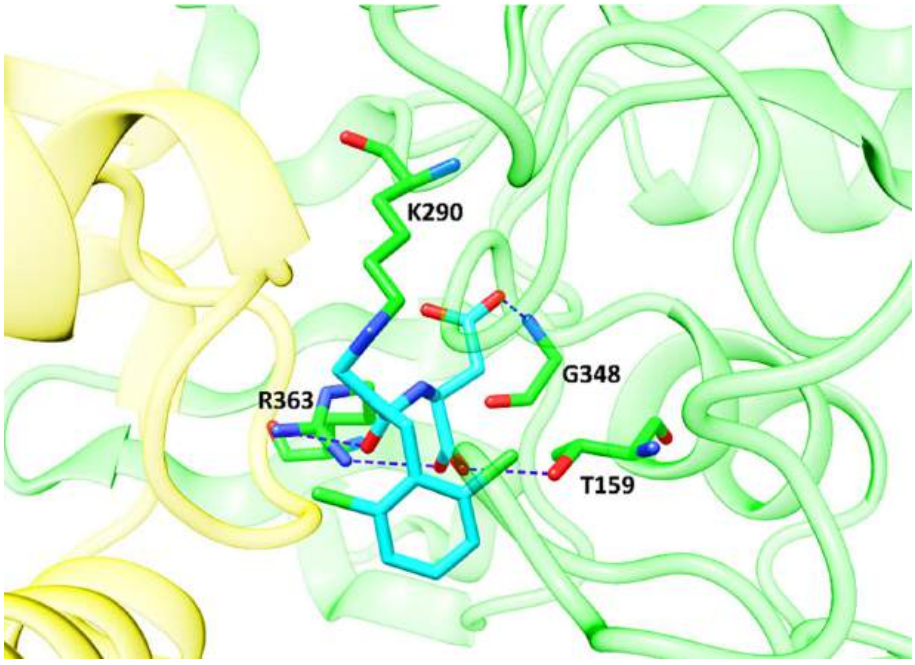

Fig. 10. Covalent adduct CM365-Lys290 obtained by covalent docking performed on the homology model of SEPT4-SEPT6 dimer. SEPT4 and SEPT6 are displayed as green and yellow cartoon, respectively. The residues involved in the interaction with the ligand are depicted as sticks. H-bonds are represented by blue dashed lines.

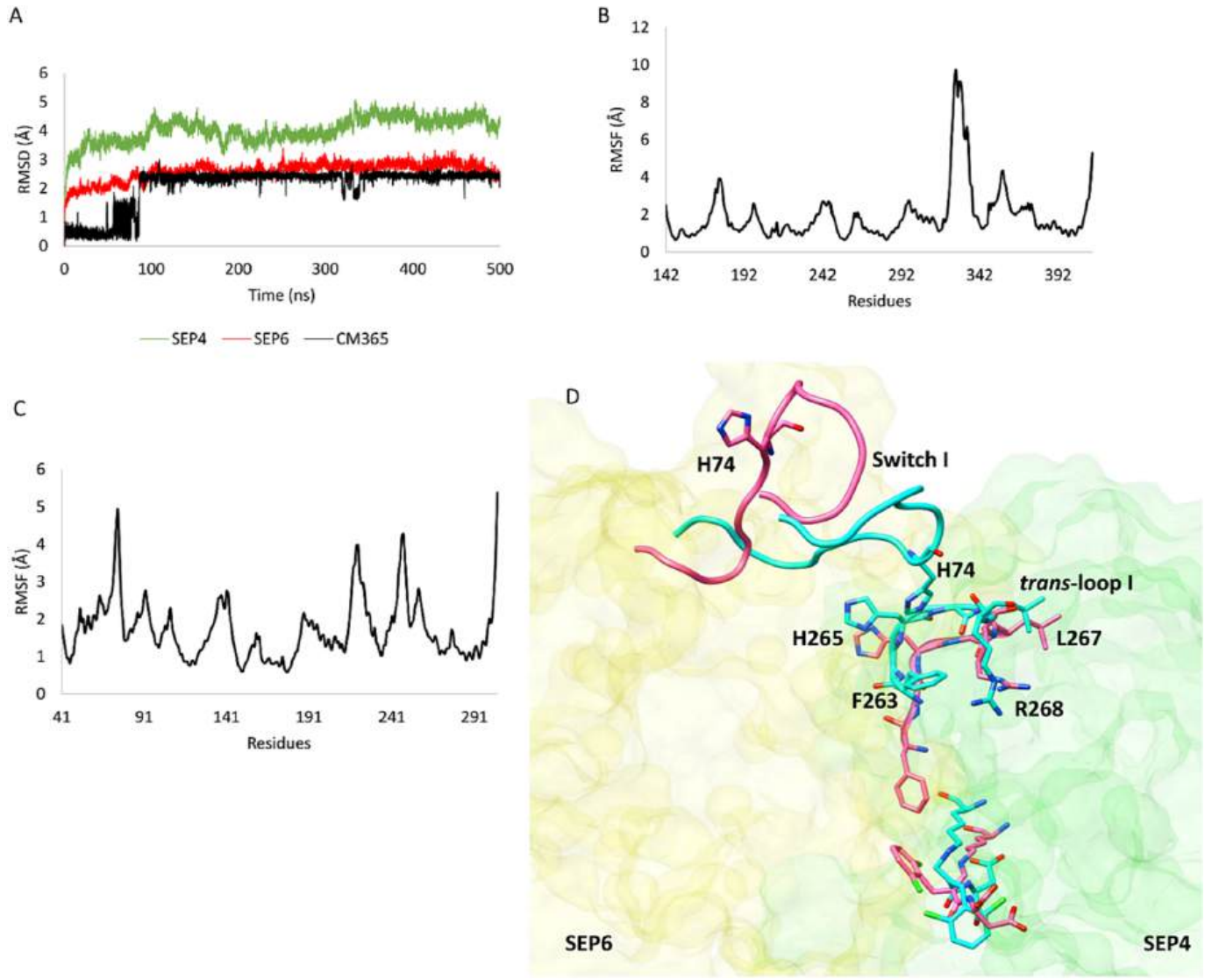

Fig. 11. A) RMSD plot of CM365 and SEPT4 and SEPT6 backbone. B) RMSF profile of SEPT4. C) RMSF profile of SEPT6. D) Representative conformations of SEPT6 switch I and SEPT4 *trans*-loop I extracted from the MD simulation (magenta) by cluster analysis, aligned on the initial coordinates (cyan).

*2.2.22. tert-Butyl N^4-(3-aminopropyl)–N2-(2-(2,6-dichlorobenzyl) acryloyl)-L-asparaginate (**23**)*

Compound **22** (0.240 g, 0.429 mmol) was dissolved in a solution of TFA (0.200 mL, 2.58 mmol) in DCM (10 mL) at 0 °C. The mixture was stirred at rt for 72 h, the mixture was cooled to 0 °C and a solution of $NaHCO_3$ (10 %, 15 mL) was added. The product was extracted with EtOAc (3 × 20 mL), dried, and concentrated under reduced pressure. The crude product was purified by silica gel chromatography (DCM/MeOH 95:5) to give **23** (0.110 g, 56 %) as a white solid. ^{1}H NMR (600 MHz, CD_3OD) $\delta = 7.36$ (d, $J = 8.2$ Hz, 2H), 7.22 (t, $J = 8.2$ Hz, 1H), 5.73 (s, 1H), 4.76–4.73 (m, two overlapping signals, 2H), 3.90 (s, 2H), 3.31–3.23 (m, 2H, partially overlapping with solvent signal), 2.97–2.90 (m, 2H), 2.80 (dd, $J = 15$, 5.4 Hz, 1H), 2.70 (dd, $J = 15$, 6.9 Hz, 1H), 1.85–1.81 (m, 2H), 1.44 (s, 9H). ^{13}C NMR (151 MHz, CD_3OD) $\delta = 172.0$, 170.3, 169.0, 140.3, 135.9, 134.4, 128.8, 128.2, 118.1, 82.0, 50.5, 36.9, 36.8, 35.7, 32.7, 27.4, 27.0.

*2.2.23. tert-Butyl N^2–(2-(2,6-dichlorobenzyl)acryloyl)-N^4-(3-(5-((3aS,4S,6aR)-2-oxohexahydro-1H-thieno[3,4-d]imidazol-4-yl) pentanamido)propyl)-L-asparaginate (**24**)*

To a stirred solution of biotine-NHS ester (0.067 g, 0.196 mmol) and DIPEA (0.033 mL, 0.196 mmol) in DMF (2 mL), **23** (0.090 g, 0.196 mmol) was added and the mixture was stirred for 5 h at rt. A solution of Na_2CO_3 10 % in water (10 mL) was added and the product was extracted with DCM (3 × 15 mL). The combined organic phases were dried and concentrated under reduced pressure. The crude product was purified by flash chromatography (DCM/MeOH 95:5 to 9:1) to give **24** (0.130 g, 95 %) as a white solid. ^{1}H NMR (600 MHz, CD_3OD) $\delta = 7.34$ (d, $J = 7.9$ Hz, 2H), 7.20 (t, $J = 7.9$ Hz, 1H), 5.72 (s, 1H), 4.74 (m, partially overlapping with HOD signal, 1H), 4.69 (t, $J = 5.9$ Hz, 1H), 4.45 (dd, $J = 7.9$, 5.2 Hz, 2H), 4.25 (dd, $J = 7.9$, 4.4 Hz, 1H), 3.90 (s, 2H), 3.28 (d, $J = 3.4$ Hz, 1H), 3.21–3.11 (overlapping signals, m, 5H), 2.87 (dd, $J = 12.6$, 4.8 Hz, 1H), 2.74–2.67 (two overlapping signals, m, 3H), 2.20–2.13 (m, 2H), 1.72–1.53 (overlapping signals, m, 6H), 1.44 (s, 9H), 1.40 (m, 2H), 1.01 (ABMX system, m, 1H). ^{13}C NMR (151 MHz, CD_3OD) $\delta = 174.8$, 171.2, 170.3, 168.8, 164.6, 140.2, 136.0, 134.5, 128.8, 128.2, 118.3, 82.1, 62.0, 60.3, 55.7, 50.5, 40, 36.9, 36.5, 36.4, 35.7, 32.8, 28.9, 28.5, 28.2, 27.3, 25.5.

*2.2.24. N^2–(2-(2,6-Dichlorobenzyl)acryloyl)-N^4-(3-(5-((3aS,4S,6aR)-2-oxohexahydro-1H-thieno[3,4-d]imidazol-4-yl)pentanamido)propyl)-L-asparagine (**25**)*

Compound **24** (0.120 g, 0.175 mmol) was dissolved in a stirred solution of TFA/DCM 10 % (20 mL). The mixture was stirred at rt for 18 h.

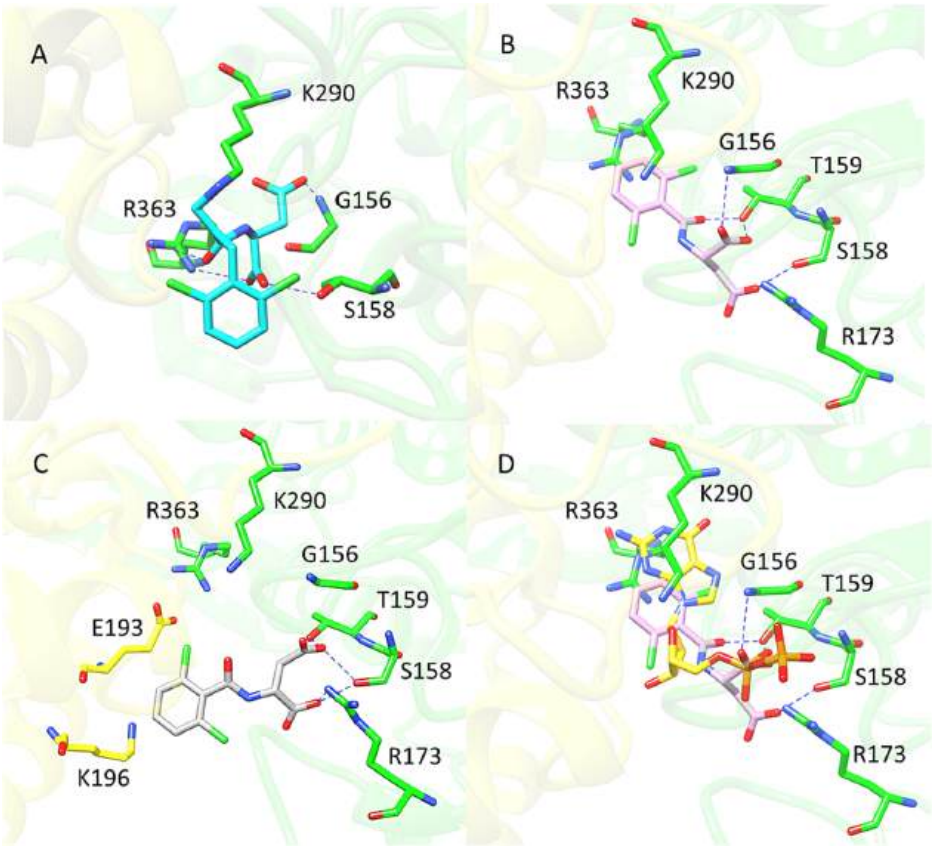

Fig. 12. Docking poses of A) CM365, B) AA6 and C) compound **6**. D) Docking pose of AA6 superimposed to the x-ray pose of GDP found in SEPT2-SEPT6 complex. H-bonds are shown as blue dashed lines.

The mixture was concentrated under reduced pressure and the crude product was purified by flash chromatography (DCM/MeOH 95:5 to 9:1) to give **25** (0.103 g, 94 %) as a white solid. ^{1}H NMR (600 MHz, CD_3OD + CD_3CN) $\delta = 7.42$ (d, $J = 8.4$ Hz, 2H), 7.28 (t, $J = 8.4$ Hz, 1H), 5.79 (t, $J = 1.8$ Hz, 1H), 4.70 (t, $J = 1.8$ Hz, 1H), 4.59 (dd, $J = 7.2$, 5.2 Hz, 1H), 4.48 (dd, $J = 7.2$, 4.4 Hz, 1H), 4.29 (dd, $J = 7.8$, 4.8 Hz, 1H), 3.99–3.92 (m, 2H), 3.23–3.16 (three overlapping signals, m, 5H), 2.92 (dd, $J = 12.8$, 4.8 Hz, 1H), 2.77 (dd, $J = 14.4$, 4.8 Hz, 1H), 2.69 (d, $J = 12$ Hz, 1H), 2.63 (dd, $J = 14.4$, 7.8 Hz, 1H), 2.24–2.17 (m, 2H), 1.75–1.54 (three overlapping signals, m, 6H), 1.46–1.40 (ABMX system, m, 2H). ^{13}C NMR (151 MHz, CD_3OD + CD_3CN) δ = 177.1, 175.9, 173.4, 169.1, 165.8, 142.1, 137.2, 136.0, 130.3, 129.6, 118.7 (overlapping with CD_3CN signal), 63.2, 61.5, 56.9, 53.6, 41.2, 40.7, 37.8, 37.7, 37.0, 34.2, 30.1, 29.7, 29.5, 26.8. MS (ESI^-): *m/z* 626/628/630 $[M-H]^-$.

2.3. Cell assays

2.3.1. Cell lines

For this study, B16-F10 melanoma, MS1 endothelial mouse cell lines and U2OS human osteosarcoma cell line were used (purchased from ATCC, Manassas, Virginia, USA). B16-F10 cells were cultured in RPMI 1640, MS1 in DMEM, and U2OS in McCoy's 5A, all of them supplemented with 10 % fetal bovine serum (FBS) and antibiotics (100 units/ml of penicillin and 100 µg/ml streptomycin) (Euroclone, Pero, Milan, Italy) in a 5 % CO_2, 37 °C incubator.

2.3.2. Cytotoxicity of compounds

Cells (1×10^3/well) were seeded in 96-well plates and incubated for 24 h. Then, they were treated with the compounds (1–100 µM) under study for 24 h. The cell proliferation reagent dimethyl thiazolyl diphenyl-tetrazolium bromide (MTT, Merck Life Science S.R.L., Roma, Italy) was used, as described by the manufacturer's protocol. Cells that had received no drug, as control, were normalized to 100 %, and the readings from treated cells were expressed as percent of viability. Four technical replicates were performed for each data point and five different experiments were run.

To evaluate cell viability at the time used in the invasion test, the crystal violet method was used. Cells (8×10^3/well) were seeded into 96-well plates and treated for 6 h with the compounds (1–100 µM) under study. Cell viability was assessed using the Crystal Violet Assay (Merck Life Science S.R.L., Roma, Italy), as previously described [27].

2.3.3. Invasion: Boyden chamber assay

In the Boyden chamber-invasion assay, 700 cells were plated onto the apical side of 50 µg/mL Matrigel (BD Biosciences, San Jose, CA, USA) coated filters (8.2 mm diameter and 0.5 µm pore size) in a serum-free medium with or without compounds (0.1–100 µM) under study. A medium containing FCS 20 % was placed in the baso-lateral chamber as a chemo-attractant. The chamber was incubated at 37 °C under 5 % CO_2. After 6 h, the cells on the apical side were wiped off with Q-tips. Cells on the bottom of the filter were stained with methanol-crystal-violet and counted (all fields of each quadrupled filter) with an inverted microscope (magnification 40 ×). The results are expressed as percentages of the inhibition of treated cells versus the control invasion measured on untreated cells. The control migration was 70 ± 4 and 86 ± 9 cells per microscope field, for U2OS and B16-F10, respectively, (number of replicates = 5).

2.3.4. Migration: Wound healing assay

In the wound-healing assay, after starvation for 18–24 h in serum-

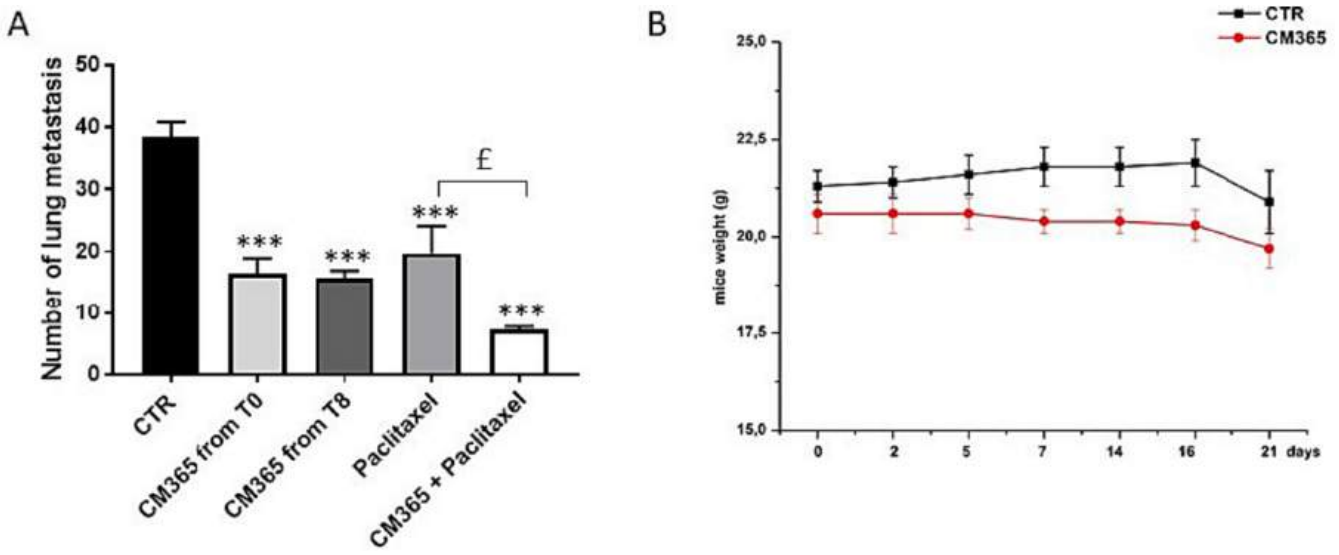

Fig. 13. In vivo inhibition of lung metastasis dissemination. A) number of lung metastasis in untreated (CTR: vehicle only i.p. for 20 days) and treated mice: CM365 12.5 mg/kg i.p. from day 0 (T0), CM365 12.5 mg/kg i.p. from day 8 (T8), paclitaxel 5 mg/kg i.v. on day 7, and CM365 (T0) + paclitaxel (T7); $^{***}P < 0.0001$ *vs* CTR; $^{£}P < 0.05$ CM365 + paclitaxel *vs* paclitaxel, One-way ANOVA Bonferroni Multiple Comparisons Test. Data are expressed as mean ± SEM ($n \geq 5$). B) weight of untreated (CTR: vehicle only i.p. for 20 days) and treated (CM: CM365 12.5 mg/kg i.p. for 20 days) mice. Data are expressed as mean ± SEM.

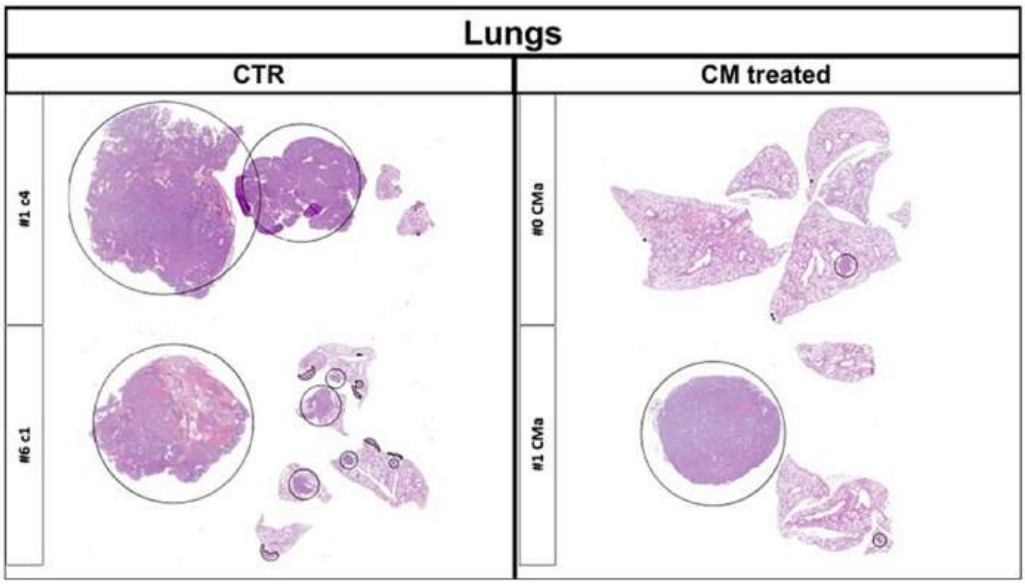

Fig. 14. Hematoxylin eosin staining of lung tumor tissue sections belonging to two representative animals (left: CTR group, right: CM365 treated group); spreading metastasis are pinpointed with black circles.

free medium, cells were plated onto six-well plates (1 x 10^6 cells/well) and grown to confluence. Cell monolayers were wounded by scratching with a pipette tip along the diameter of the well, and they were washed twice with serum-free medium before their incubation with the compounds under study (1 and 30 μM). In order to monitor cell movement into the wounded area, five fields of each wound were photographed immediately after the scratch (T0) and after 24 h.

2.3.5. Adhesion of B16-F10 on MS1 endothelial cells

MS1 were grown to confluence in 24-well plates, washed and rested for 1 day in DMEM plus 10 % FCS. Then, they were incubated with 10 ng/ml mouse TNF-α and increasing concentrations of the compounds under study (0.01–10 μM) for 18 h, washed with fresh medium twice and incubated for 45 min with the tumor cells (7×10^4 cells per well). After incubation, non-adherent cells were removed by being washed three times with DMEM. The centre of each well was analysed by fluorescence image analysis. Adherent cells were counted by the Image Pro Plus Software for micro-imaging (Media Cybernetics, version 5.0, Bethesda, MD, USA). Single experimental points were assayed in triplicate. Data are shown as percentages of the inhibition of treated cells versus the control adhesion measured on untreated cells; this control adhesion was 83 ± 5 cells per microscope field ($n = 5$).

2.3.6. Protein extraction and Western blot analysis

B16-F10, MS1 and U2OS cells were seeded in 75-cm^2 flasks and treated as indicated. Subsequently, the cells were harvested, washed once in ice-cold isotonic buffer Phosphate-buffer saline (PBS 1x), pH 7.4, and resuspended in a lysis buffer composed of 20 mM Tris–HCl pH 7.4,

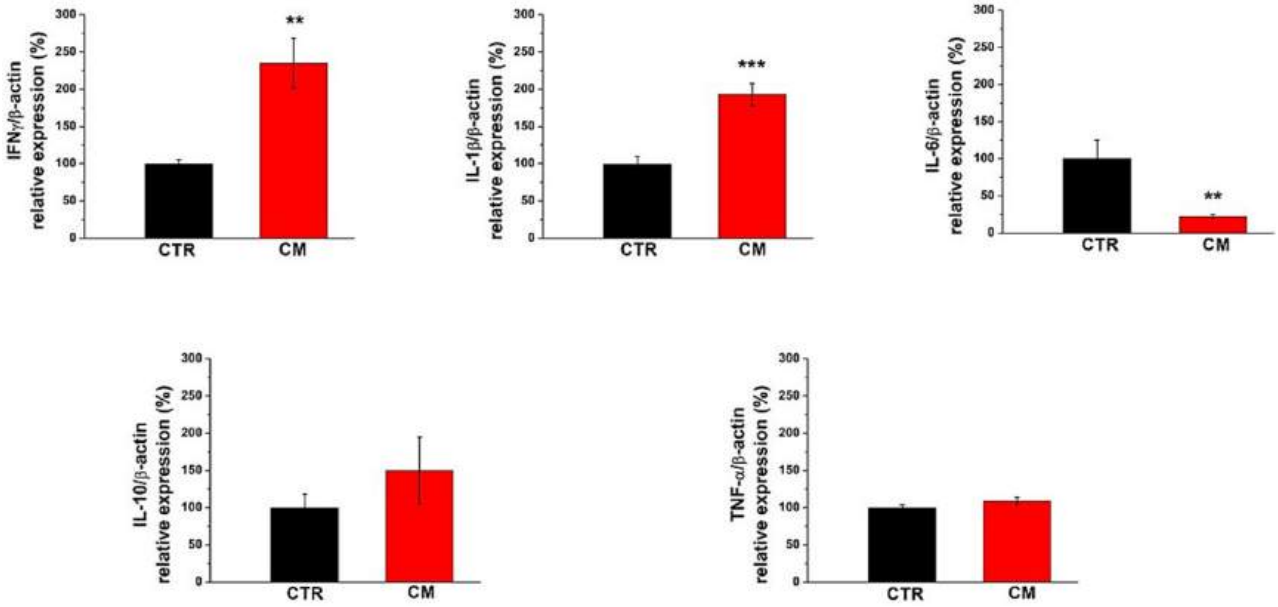

Fig. 15. *Ex vivo* cytokine pattern expression in untreated (CTR) and treated (CM365) mice assessed in the lung by Real Time PCR. **P < 0.01 *vs* CTR; ***P < 0.005 *vs* CTR, Mann-Whitney test.

150 mM NaCl, 5 mM EDTA, 1 % v/v Triton X-100, P2850 phosphatase, and P8340 protease (inhibitor cocktails Merk Life Science S.r.L., Milan, Italy). The samples were incubated for 15 min at 4 °C and then centrifuged at 10,000 rpm for 15 min at 4 °C. The supernatants were collected, and the protein concentration was determined using a commercially available Bio-Rad protein assay reagent (Bio-Rad Laboratories, Hercules, CA, USA).

Western blot analysis was performed using home-made 9.3 % SDS–polyacrylamide gels (SDS-PAGE) or 5–15 % gradient SDS–PAGE precast gels (Bio-Rad Laboratories). Twenty to forty μg of proteins were mixed with the sample-loading buffer (50 mM Tris-HCl pH 6.8, 100 mM dithiothreitol, 2 % SDS, 0.1 % bromophenol blue and 10 % glycerol), followed by heat-denaturation for 5 min at 95 °C using a thermoblock. The protein samples were then resolved by SDS-PAGE. The run was performed at the constant voltage of 100 V. The proteins were then transferred onto a nitrocellulose membrane with a semidry transfer apparatus (Trans-Blot Turbo Transfer System semi-dry, Bio-Rad Laboratories). The membranes were subsequently blocked for 1 h with 5 % non-fat dry milk dissolved in Tris-buffered saline (TBS)–Tween 20, incubated overnight at 4 °C with primary antibodies, washed three times with TBS–Tween 20, and incubated with HRP-conjugated secondary antibodies (Bio-Rad Laboratories) for 1 h at room temperature. Primary antibodies used were as follows: β-actin (sc-47778, Santa Cruz Bio), septin-4 (12476-1-AP, Proteintech, Manchester, UK). The detection of the bands was carried out after the chemiluminescence reaction with ECL and visualized using a Bio-Rad visualizer (Bio-Rad Molecular Imager, ChemiDoc XRS+, Bio-Rad Laboratories, Hercules, CA, USA).

2.4. Target identification

2.4.1. Intracellular accumulation

Intracellular accumulation of compounds AA6 and CM365 was measured on B16-F10 cells grown in 100-mm diameter Petri dishes. Confluent cells were incubated for 4 h in fresh medium containing 50 μM AA6 or CM365, washed twice in ice-cold PBS and detached with scraper. Cells were centrifuged for 5 min at 200 *g* (4 °C) and resuspended in 0.5 mL of lysis buffer (TRIS 50 mM; KCl 100 mM; $MgCl_2$ 5 mM; EDTA 1 mM). After centrifugation for 3 min at 3000 *g* (4 °C), the supernatant (cytosolic fraction) was collected. The amount of cell proteins was measured by the Brønsted-Lowry method in 50 μl of supernatant, the remaining part was stored at −80 °C until analysis. The mitochondria pellet was washed and resuspended in 320 μl of resuspension buffer (Sucrose 250 mM; K_2HPO_4 15 mM; $MgCl_2$ 2 mM; EDTA 0.5 mM); the amount of cell proteins was measured in 40 μl of supernatant, the remaining part was stored at −80 °C until analysis. Before analysis, the samples were treated with CH_3CN 1:1, filtered and then analysed by an Acquity Ultra Performance LC (Waters Corporation Milford MA, USA), equipped with BSM, SM, CM and PDA detectors. The analytical column was a Zorbax Eclipse XDB-C18, 150 × 4.6 mm × 5 μm. The mobile phase consisted of CH_3CN 0.1 % HCOOH/H_2O 0.1 % HCOOH 25/75 v/v. UPLC retention time (t_R), was obtained at flow rates of 0.5 $mLmin^{-1}$ and the column effluent was monitored using a Micromass Quattro micro API Esci with multi-mode ionization enabled, as the detector. The molecular ions $[M-H]^-$ were used for the quantitative measurements of the analyte. MS conditions were as follows: drying gas (nitrogen), heated at 350 °C at a flow rate of 800 Lh^{-1}; nebulizer gas (nitrogen), at 80 Lh^{-1}; capillary voltage in negative mode at 3000 V; fragmentor voltage at 30 V. The values obtained from the integration of compound peaks were interpolated into calibration curves obtained using standard solutions at 0.1 μM to 100 μM ($r^2 = 0.996$). The quantity of compounds in the mitochondrial and cytosolic fractions was expressed as pmol/mg protein.

2.4.1.1. Cell surface protein labelling. Confluent 1 × 10^7 B16-F10 cells were incubated for 4 h in fresh medium containing 10 μM **25**, or vehicle alone (DMSO). Cells were washed twice in ice-cold PBS and detached with scraper. Cells were centrifuged for 5 min at 1000*g* (4 °C), resuspended in 2 mL of PBS with ExtrAvidin®-FITC 25 μg/mL (Merck, Darmstadt, Germany), and incubated for 45 min (4 °C) with slow shaking. Then, cells were centrifuged for 5 min at 1000*g* (4 °C), and washed three times in ice-cold PBS. The membrane proteins were isolated with the ProteoExtract® Transmembrane Protein Extraction Kit (Millipore, Merck, Darmstadt, Germany), following the manufacturer instructions. The amount of cell proteins was measured by the Brønsted-Lowry method. The cytosolic fractions and the membrane protein fractions were checked for the FITC-associated fluorescence using an EnSight® multimode plate reader (Perkin Elmer, Waltham, Massachusetts).

2.4.1.2. Proteomic analysis. Confluent B16-F10 cells were incubated for 18 h with CM365 10 μM or DMSO (vehicle). The cytosolic fractions and the membrane protein fractions were isolated as previously described, and stored at −80 °C until analysis.

SDS-PAGE analysis (reducing conditions) - The protein content of cytosolic and membrane protein fractions, prepared as described above, was measured by Bradford Assay, according to the manufacturer's specifications.

30 μg of protein material (wet weight) was dissolved in *Laemmli* sample buffer with 50 mM DTT and heated at 95 °C for 5 min. SDS-PAGE analysis was performed using precast gels placed in the Mini-PROTEAN Tetra electrophoretic cell filled with running buffer, and specifically the electrophoretic run was conducted at 150 V (constant). Post-run, the gel was immersed in ultrapure water to remove any trace of running buffer and then stained for 1 h with Bio-Safe Coomassie. After removing the stain excess in ultrapure water (2 h, under shaking) the images of gels were acquired using the ChemiDoc Imaging Systems (Bio-Rad Laboratories, Inc).

In-gel tryptic digestion - Each band selected from the whole lane (11 bands) was cut using a scalpel, finely chopped, transferred to a new low-binding eppendorf, destained and proteolytically digested as reported by Marchis, Altomare at al. [28]. In particular, after reducing and alkylating protein disulfide bonds, 1 μg of trypsin, dissolved in digestion buffer (ammonium bicarbonate 50 mM) at a final concentration of 5 ng/μl, was added to the gel portions and incubated overnight at 37 °C in the thermomixer, set for gently shaking at 450 rpm. The tryptic peptide mixtures were acidified with formic acid up to a final concentration of 1 % (v/v), and to guarantee better protein detection, an additional peptide extraction step was performed as previously described [28]; at this point, the extracted peptide fractions collected were clean-up by using the so-called zip-tip devices (nominal binding capacity of 6 μg), dried in the SpeedVac (Martin Christ., Osterode am Harz, Germany) at 37 °C and stored at −20 °C until the nLC-HR-MS/MS analysis.

nLC-HR-MS/MS analysis (Orbitrap Elite™ Mass Spectrometer) - Peptide mixtures, resuspended in a proper volume (20 μl, enough for two technical replicates) of 0.1 % TFA mobile phase, were analyzed using a Dionex Ultimate 3000 nano-LC system (Sunnyvale CA, USA) connected to the Orbitrap Elite™ *Mass Spectrometer* (Thermo Scientific, Brema, Germania) equipped with an ionization source, the *Nanospray Ion Source* (Thermo Scientific Inc., Milano, Italia), by applying a nLC-HR-MS/MS method previously set-up and reported by Baron et al. [29].

Targeted data analysis - Proteome Discoverer software (version 2.2.0.338, Thermo Fisher Scientific, USA), designed to computationally process full and tandem mass spectra, was used to reprocess MS raw data. The experimental mass spectra matching against theoretical ones, in turn obtained by the *in silico* digestion of the *Mus Musculus* proteome database (https://www.uniprot.org/), is achieved by means of the SEQUEST algorithm, developed to automatically cross-validate the PSMs (peptide spectral matches) generated.

For the targeted analysis, aimed at characterizing potential covalent protein adducts with CM365 involving nucleophilic aminoacidic sites exposed by membrane proteins, specific experimental parameters were listed in the processing workflow with regard to the instrument setup for high-resolution MS acquisition: mass range between 350.0 Da − 5000.0 Da, any activation type mode, total intensity threshold 1, S/N threshold 5, 5 ppm as precursor mass tolerance, and 0.5 Da as fragment mass tolerance; trypsin was set as the proteolytic enzyme and 2 was the number of missed cleavages; carbamidomethyation of cysteine (+57.021 Da) was set as fixed modification while the oxidation of methionine (+15.995 Da) as variable modification. Furthermore, the mass shift considered plausible according to the speculated reaction mechanism was also included as variable modification targeting the nucleophilic moieties of Cys and Lys (+344.0092502 Da), of which the structural formulae are reported in Scheme 1.

To ensure the lowest number of false positives, the mass values experimentally recorded were further processed through a combined search with the Decoy database, where the protein sequences are inverted and randomized. This operation allows the calculation of the false discovery rate (FDR) for each match, so that all the proteins out of range of FDR between to 0.01 (strict) and 0.05 (relaxed) were rejected. Once the task of matching with the *UniProt*.database was completed, the resulting protein list was filtered under stringent conditions to ensure the lowest error probability (0.5 %), and all the PSMs of interest were manually checked and validated.

2.5. Computational studies

2.5.1. Homology modelling

The 3D structure of septin-4 (SEPT4) was obtained by homology modelling performed by means of SWISS-MODEL webserver [30] (https://swissmodel.expasy.org/). The primary sequence of SEPT4 was retrieved form *Uniprot* database [31] (ID O43236) and used as input for the template search. The structure of septin-2 (SEPT2) in complex with septin-6 (SEPT6) (PDB ID 6UPA) which showed GMQE of 0.47 and sequence identity of 65.09 % was selected as template for the model building. The resulting structure was validated by generating the Ramachandran plot using PROCHECK tool [32], which revealed that the 89.3 % and 9.8 % of the residues are in the most favored and additional favored regions, respectively. The generously allowed and disallowed regions contained one residue, respectively. By aligning the so generated monomer of SEPT4 with the SEPT2-SEPT6 complex, a model of SEPT4-SEPT6 dimer was obtained. The resulting complex was protonated by means of VEGA ZZ program [33] and optimized by 10,000 steps of energy minimization keeping the backbone fixed to preserve the original folding.

2.5.1.1. Molecular docking. The obtained homology model of SEPT4-SEPT6 complex was used to perform covalent docking by means of GOLD v2020.1 software [34]. Ligand structure was built by VEGA ZZ program as reported elsewhere [35]. The binding site was set in order to include the residues within 10 Å from Lys290 and ten poses were generated. The "allow early termination mode" was unchecked and the poses with RMSD values lower than 1 Å were clustered together. The highest scored pose was chosen for the following studies. A standard docking protocol using the same settings reported above was applied to analyze the binding modes of compounds **1** and **6**.

2.5.1.2. Molecular dynamics. Molecular dynamics simulation was performed by using the software AMBER 18 [36]. Amber ff14SB force field [37] was employed for protein parametrization, while the General Amber Force Field (GAFF) [38] was used to parametrize the ligand. Partial charges for the covalent inhibitor including Lys290 were computed based on the RESP method at HF/6-31G* level by means of Gaussian 16 [39]. The protocol used to run the simulation has been described elsewhere [29]. The cpptraj module [40] of AMBER18 was used for RMSD and RMSF analysis, while trajectory clustering was performed by means of TTClust [41] tool as reported in [42].

2.6. In vivo studies

Animals were handled in accordance with recognized guidelines on experimentation; the "3 Rs" policy (99/167/EC: Council Decision of 25/1/99) of Replacement by alternative methods, Reduction of the number of animals and the Refinement of experiments has been fully applied. Animals were bred in the animal facility of the Department of Health Sciences (UPO, Novara, Italy). All experimental procedures were done according to Europeans Guidelines and our Institution's ethics commission. The study was approved by the Bioethics Committee for Animal Experimentation of Ministero della Salute, Rome (authorization n° 274/2022-PR; Risp. a prot. DB064.79).

2.6.1. Lung metastasis mouse model of melanoma

Six to eight-week-old female C57BL/6J mice (Charles River Laboratories, Wilmington, MA, USA) were injected intravenously (iv) with B16-F10 cells (5×10^5 cells/mouse). After 1 h from the cell tumor injection (T0), mice were randomized in a blind fashion into homogenous groups (15 mice per group, 3 independent experiments in total) and assigned to different treatments: 1- control group, CTR, injected intraperitoneally (ip) with the vehicle used to solubilize the compound, a mix of EtOH and Cremophor EL (1:1, v/v), diluted in NaCl 0.9 %; 2- treated group, injected daily i.p. with CM365 (12.5 mg/kg) until day 20. Each mouse received 21 injections, in total, for 21 consecutive days of treatment (Fig. 2A). Treatment-related toxicity was monitored by checking mouse weight at day 0, 2, 5, 7, 14, 16, 21.

In another set of experiments, 5 mice per group were assigned to 3 different treatments (Fig. 2B): 1-treated group, injected i.v. with paclitaxel (5 mg/kg) on day 7; 2-treated group, injected i.p. with CM365 (12.5 mg/kg) every day, starting from the day 8 until day 20; 3-treated group, injected i.p. with CM365 (12.5 mg/kg) every day, starting from day 0 until day 20, and i.v. with paclitaxel (5 mg/kg) on day 7.

2.6.1.1. Real-Time RT-PCR. Total RNA was isolated from the lungs of the mice (CTR *vs* CM) and collected at the end point, using TRIzol reagent (Invitrogen). RNA (500 ng) was retrotranscribed using the QuantiTect Reverse Transcription Kit (Qiagen, Hilden, Germany). IFN-γ, IL-6, IL-1, TNF-α, IL-10, IL-17A, and IL-21 expression were evaluated with a gene expression assay (Assay-on Demand, Applied Biosystems, Foster City, CA, USA). The β-actin gene was used to normalize the cDNA amounts. Real Time PCR was performed using the CFX96 System (Bio-Rad Laboratories) in duplicate for each sample in a 10 μl final volume containing 1 μl diluted cDNA, 5 μl TaqMan Universal PCR Master Mix (Applied Biosystems), and 0.5 μl Assay-on Demand mix. The results were analyzed with a Delta-Delta CT method.

2.6.1.2. Histological analysis. At the end point (T21), lungs of all the animals sacrificed were embedded in paraffine and stored at −20 °C until use. The samples were cut using a microtome (Leica RTM 2125 RTS) in 2 μm tissue sections. Hematoxylin Eosin staining (H&E) was performed using an automatic staining machine (Leica ST5020) available in the Department of Medical Science of Molinette Hospital in Turin (Anatomo-Patology section). Images of the sections were acquired using NDP. View2 software at 20 × magnification.

2.6.1.3. Statistical analysis. Data are shown as mean ± SEM. Statistical analyses were performed with Prism 5.0 software (GraphPad Software, La Jolla, CA, USA) using one-way ANOVA, Bonferroni Multiple Comparisons Test.

3. Results

3.1. Synthesis

In the first set of compounds (derivatives **2**–**6**), we modulated the aspartic acid moiety by replacing the β-positioned carboxylic group with residues typical of natural aminoacids endowed with different properties. This modulation was performed to determine the importance of the β-substituent and the preferred physico-chemical properties of the substituent. Therefore, we introduced a lipophilic residue (compound **2**), a weakly basic residue (compound **3**), a strongly basic residue (compound **4**) and an amide (compound **5**) in position β to the aminoacidic portions of the molecule. The importance of the spatial orientation of acid substituents around the chiral center was studied through the synthesis of compound **6**, the R-stereoisomer of AA6. Further modulation of the aspartic acid moiety was performed by elimination of the β-carboxylic group (compound **7**), methylation on the amide nitrogen (compound **8**), and homologation of the side chain (compound **9**). The 2,6-dichlorobenzene ring in compound **1** (AA6) was also substituted in position 4 with a phenyl group (compound **11**) to verify whether this position can accommodate bulky lipophilic substituents. In compounds **12** and **13**, a spacer of one or two carbon atoms was introduced between the 2,6-dichlorobenzene ring and the amide, and a double bond conjugated with the amide group forming an acrylamide substructure was inserted in compounds **18** and **19**. Finally, a biotinylated probe (compound **25**) was synthesized for mechanistic studies.

Dichlorobenzoic acid derivatives **1**–**13** were synthesized according to the procedure reported in Schemes 2 and 3. For the synthesis of compounds **1**–**5**, dichlorobenzoic acid was converted into the corresponding benzoylchloride and then reacted with the appropriate amino acid in basic water to afford the desired compounds **1**–**5** in modest yields (38–47 %) according to published procedures [19,22]. For the synthesis of compound **6**, the (R)-enantiomer of **1** (AA6), the coupling of the benzoyl chloride with di-*tert*-butyl protected-(R) aspartic acid was executed in dry DMF using diisopropylethylamine (DIPEA) as the base. Removal of the protecting groups with 10 % trifluoroacetic acid in dichloromethane (DCM) allowed the obtainment of desired compound **6** in higher yields (97 %) avoiding the use of strongly basic aqueous medium. A similar procedure was then applied to obtain compounds **7**–**9**. The coupling was performed using the ethyl ester of glycine, sarcosine and β-alanine, respectively. In this case, the final hydrolysis was performed in basic medium (Scheme 2).

The synthesis of compound **11** was performed using a similar strategy starting from 4-bromo-2,6-dichlorophenylacetic acid (Scheme 3). After activation of the acid with thionyl chloride and coupling of the acyl chloride with di-*tert*-butyl protected-(S) aspartic acid, the desired intermediate **10** was obtained in good yields. This intermediate was submitted to a Suzuki reaction with phenylboronic acid and palladium tetrakis triphenylphophine as the catalyst to obtain the 4-phenyl substituted derivative which, after chromatography, was deprotected in TFA 10 % in dichloromethane to afford compound **11** in 66 % yields over two steps. The synthesis of compounds **12** and **13** was performed using 2,6-dichlorophenylacetic acid or 3-(2,6-dichlorophenyl)propionic acid as the starting materials (Scheme 3). Hydroxybenzotriazole (HOBt), N,N,N′,N′-Tetramethyl-O-(1H-benzotriazol-1-yl)uronium hexafluorop hosphate (HBTU)-mediated coupling of the acids with di-*tert*-butyl-protected (S)-aspartic acid using diisopropylethylamine as the base in dry DMF afforded the protected amides that were deprotected as described above to give the final compounds **12** and **13** in good yields.

For the synthesis of the final compounds **18** and **19** (Scheme 4), the preparation of acrylic acid derivative **16** was required. To synthesize this intermediate, we relied on a previously developed procedure [26] employing a Horner-Emmons reaction with *tert*-butyl diethylphosphonoacetate to obtain **14**; then, base-promoted reaction with paraformaldehyde afforded intermediate **15** which was treated with trifluoroacetic acid to give desired acrylic acid **16** in good overall yield. The HBTU/HOBt-mediated coupling with di-*tert*-butyl L-aspartic acid or dimethyl L-aspartic acid furnished the protected intermediate **17** and the desired **18**, respectively. Finally, the acidic treatment performed on **17** furnished the desired compound **19** (CM365).

To obtain the biotinylated probe **25**, the synthetic route depicted in Scheme 5 was used. The commercially available Fmoc-L-aspartic acid 4-*tert*-butyl ester was coupled with *N*-Boc-diaminopropane using carbonyldiimidazole (CDI) as the activating agent to give derivative **20**. Deprotection of the Fmoc-protected amino group allowed the obtainment of **21** which was reacted with the acyl chloride of compound **16** to afford the di-protected intermediate **22**. The selective deprotection of the carbamate was performed by using three molar equivalents of TFA in DCM to obtain compound **23**, bearing a free terminal amino group. This intermediate was reacted with commercially available biotin-NHS ester in basic medium to afford **24** which was then deprotected in the usual way to produce the desired compound **25**.

3.2. Cell assays

3.2.1. Invasion assay in B16-F10 cells

The new compounds were first tested for their inhibitory activity on tumor cell invasion. B16-F10 cells were plated in Transwell Boyden chambers in the presence of the compounds at concentrations ranging from 0.1 to 100 μM. These concentrations were not toxic (see Supporting Material, Figs. S1, S2). The compounds showed heterogeneous inhibitory activities, ranging from the inactivity of compounds **6** and **18** to the remarkable inhibition of invasiveness of compounds **1** (AA6), **5**, **13** and **19** (CM365) as illustrated in Table 1 and Fig. 3. Also the probe compound **25** showed a good efficacy in invasiveness inhibition. For the most active compounds (maximal efficacy at 100 μM > 50 %), the IC_{50} values were calculated and are shown in Table 1.

3.2.1.1. Migration assay in B16-F10 cells. The inhibition of B16-F10 cells migration was also assessed with the wound healing assay for two selected compounds, namely AA6 and CM365, selected because of their good efficacy in *in vitro* invasiveness inhibition, but different predicted interaction with the target, non-covalent for AA6 and covalent for CM365. After scratching the confluent monolayer of B16-F10 cells, cells were treated with vehicle, AA6 (1 and 30 μM) or CM365 (same concentrations). As shown in Fig. 4, cell migration was inhibited by both the compounds, even at the lower concentration tested.

3.2.2. B16-F10 cells adhesion to MS1 endothelial cells

Compounds AA6 and CM365 were also used to assess the effects on cell adhesion. In particular, we analysed the effects of AA6 and CM365 (0.01–10 μM) on adhesion of B16-F10 cells to MS1 endothelial cells. As shown in Fig. 5, both compounds inhibited cell adhesion in a concentration-dependent manner, with IC_{50} values of 0.16 ± 0.02 μM and 0.086 ± 0.02 μM, respectively.

3.3. Target identification

3.3.0.1. Intracellular accumulation and cell surface protein labelling

In order to identify the cellular target of compound AA6, we first investigated the intracellular distribution of AA6 and its reactive derivative CM365, potentially capable of forming a stable bond with the target. After incubation, neither compound was detected in the cytosolic nor in the mitochondrial fractions of B16-F10 cells (Table S1, Supplementary Material), thus excluding that the target was inside the cell. Next, we synthesized the biotinylated analogue of CM365, compound **25**, in order to verify the formation of covalent membrane protein adducts, after incubation with B16-F10 cells. The cytosolic fraction obtained from B16-F10 cells treated with **25** or vehicle, washed and then incubated with ExtrAvidin®-FITC, showed the same FITC-associated fluorescence confirming the inability of the compound to penetrate inside the cell. On the contrary, the fluorescence measured in the membrane fraction derived from cells treated with **25**, washed and finally incubated with ExtrAvidin®-FITC was about twice that measured in the membrane fraction obtained from cells treated with vehicle only (Table S2, Supplementary Material). These results confirmed that compound **25** and, likely, CM365 bind covalently to the target cell surface and support the possibility that the effects exerted by AA6 and its derivatives may be mediated by binding to a protein on the cell membrane.

3.3.1. Targeted identification of CM365 covalent protein adduct(s) by nLC-HR-MS/MS analysis (proteomics).

The SDS-PAGE profiles in reducing conditions of cytosolic and membrane protein fractions are shown in Fig. 6: each lane is characterized by a fairly heterogeneous profile with good bands' definition, distributed over the entire molecular weight range; actually, here the SDS-PAGE is not applied for an analytical purpose, but to merely fractionate the entire proteome in 11 sub-fractions (A-N), reducing the amounts of peptides to be analyzed in each data dependent LC-MS run, and thus increasing the rate of peptide identification.

With the intent of localizing the formation of covalent adducts on key membrane protein residues targeted by CM365, experimental MS spectra were processed by selectively 'tracing' on the nucleophilic residues (i.e. cysteine and lysine) the mass shift values (Δm) ascribable to the formation of the most representative CM365-adducts. Firstly, data processing confirmed the potential of the method used in comprehensively profiling protein fractions: the analysis led to a good characterization in terms of peptides sequenced on the basis of the validated PSMs, and thus of the number of proteins (Table 2).

Besides, the automatic matching tasks (*Proteome Discoverer* software) provided a list of PSMs, grouped by sequence homology, bearing plausible covalent adducts; for each peptide adduct' assignment, the best experimental fragmentation spectra were manually checked for concordance with the theoretical *in silico*-simulated fragmentation pattern: a peptide adduct can be confirmed only when the fragmentation spectra show b and/or y fragment ions flanking the modified residue. After a rigorous evaluation of the reports output by the *Proteome Discoverer* software, one stable conjugate was clearly and unequivocally identified. Below is reported the fragmentation spectra that clarifies the identification of the modified peptide, whose sequence includes a central lysine residue bearing the adduct, belonging to the protein Septin-4 (ID: P28661).

The fragmentation spectra of the peptide with sequence VNIVPILA-**k***ADTLTPPEVDRK bearing the CM365 adduct on Lys290, indicated with an asterisk, is shown in Fig. 7 (experimental condition M_CM_100μM, namely referred to the 100 μM CM365 treated membrane protein fraction); precisely, the target residue is covalently conjugated to the reactive molecule via *Michael addition.* The fragmentation spectra of the precursor ion $[M + 3H]^{3+}$ having *m/z*: 878.44824 is characterized by almost all the fragments belonging to the *y/b*-series, together with the immonium ion corresponding to the sole Lys bearing the adduct (445.11658 Da), overall confirming the assignment, with an XCorr value of 2.86.

A target-based approach was used to further investigate the experimental condition M_CM_100μM (100 μM CM365 treated membrane protein fraction), in order to confirm with good confidence the formation of the stable CM365-conjugate involving *Septin-4* (Lys290); specifically, the peptide with sequence VNIVPILAk*ADTLTPPEVDRK, bearing the adduct on the Lys marked with an asterisk, was manually inspected by (i) extracting the single ion trace (SIC or XIC) of the peptide in the + 2 (*m/z* 1317,16706), +3 (*m/z* 878,447132), +4 (*m/z* 659,087168) charge states (Fig. 8A); and (ii) by manually interpretating the fragmentation spectra of the target peptide (modified*) (Fig. 8B).

3.3.2. Septin-4 protein expression in B16-F10 cells and invasion assay in septin-4 lacking cells.

To verify the presence of septin-4 in B16-F10 cells and the absence of CM365 effects on septin-4 expression, a western blot analysis was performed on B16-F10 cells treated or not with CM365 (30 μM). An identical analysis was performed also on human bone osteosarcoma epithelial (U2OS) cells, which do not express septin-4 [43]. The results reported in Fig. 9A confirmed the presence of the protein target in B16-F10 cells, with no changes in septin-4 expression after compound incubation. As expected, no septin-4 was detected in U2OS cells, even after CM365 incubation (Fig. 9B). Since AA6 and CM365 inhibited cell adhesion to endothelial cells after incubation of MS1 cells with both compounds, the presence of septin-4 in MS1 cells was verified and confirmed as well, as reported in Supplementary Material (Fig. S3).

In order to confirm the target identification, we further investigated the effect of CM365 on invasiveness in U2OS cells, which do not express septin-4 (Fig. 9B). U2OS cells were plated in the Transwell Boyden chamber and treated with CM365 at concentrations ranging from 0.1 to 30 μM. As shown in Figure S4, none of the concentrations tested

significantly inhibited U2OS cells invasiveness.

3.4. Computational studies

To further study the interaction of CM365 with its target, the covalent adduct between Lys290 of SEPT4 and CM365 was simulated by covalent docking by means of the software GOLD. SEPT4 belongs to the SEPT2 subgroup which are known to polymerize with the SEPT6 subgroup members (SEPT6, 8, 10, 11) through their G-interface which includes the guanine nucleotide-binding site [44]. Lys290 is a conserved residue among the SEPT2 subgroup members; it is located at the GTP binding site and establishes a H-bond with the ribose moiety of the nucleotide. In the experimental structures of SEPT2 in complex with the SEPT6 subgroup members, the corresponding lysine residue, Lys183, is able to engage SEPT6 interface forming a H-bond with a conserved proline residue of the *trans* loop I, thus contributing to the contact surface between the two protein partners [45].

Considering that no experimental structure is currently available for SEPT4, a model of SEPT4-SEPT6 dimer was generated by homology modelling as detailed under Material and Methods section, and the obtained structure was employed for docking analysis. As shown in Fig. 10, the results suggested that one of the carboxyl groups of CM365 might form a salt bridge with Arg363 and a H-bond with the side chain of Thr159. Instead, the other carboxyl group could be involved in H-bond with Gly348, while the carbonyl group might elicit a H-bond with Arg363. Finally, one of the chlorine atoms might establish a halogen bond with Thr159.

The effect of the covalent adduct formation on the stability of SEPT4-SEPT6 dimer was investigated by performing 500 ns of MD simulations using the complex gained from the covalent docking as starting coordinates. The stability of the system was evaluated by computing the RMSD of both proteins and ligand. As depicted in Fig. 11A, SEPT6 showed a more stable behavior if compared to SEPT4 for which RMSD values of about 4 Å were registered. CM365 displayed some fluctuations at the beginning of trajectory becoming stable at about 100 ns. The flexibility of the single residues was evaluated by computing the RMSF values. As results, we observed that the most flexible region of SEPT4 was detected around residue 329 (Fig. 11B), which is located in an extended loop containing the polyacidic region (PAR) of septins which is involved in the NC-interface [44]. Instead, the highest fluctuations for SEPT6 were observed around residues 69–77 (Fig. 11C) which belong to the switch I region that is crucial for the engagement of SEPT2 subgroup members such as SEPT4. In more details, the switch I of SEPT6 contributes to determine the selectivity at the G-interface as it elicits some specific interactions involving characteristics residues of the switch I of SEPT6 subgroup members and the *trans*-loop I of SEPT2 subgroup members. One of such residues is His74 of SEPT6 switch I which occupies a pocket lined by the residues from Phe263 to Arg268 of the *trans*-loop I of SEPT4 (Fig. 11D) [45]. Phe263, which is characteristics of SEPT2 members, determines the conformation of this pocket [44]. Interestingly, during the MD simulation, this residue approaches the aromatic rings of CM365 causing a rearrangement of the pocket and a different orientation of switch I, thus leading to the reduction of the contact surface between SEPT4 and SEPT6 (Fig. 11B). Other positional fluctuations detected for SEPT6 regards residues 218–224 located in the PAR containing loop, and the region around residue 247 belonging to the Septin unique element (SUE) which seems to be involved in the filament formation at both G and NC-interfaces [46].

Overall, the obtained outcomes suggested that the above described structural changes induced by the covalent adduct at the interface between the two proteins might be responsible for the inhibition of SEPT4 function.

In order to extend these observations to the other compounds of the series, the binding mode of derivatives **1** (AA6), effective in inhibiting B16-F10 cells invasiveness, and **6**, not inhibiting B16-F10 cells invasiveness, was investigated by docking simulation by means of the software GOLD. Considering that these compounds lack the reactive portion of CM365 responsible for the covalent adduct formation, a standard docking protocol was applied. The outcomes revealed that both the compounds are able to form hydrogen bonds with T159 through their amide carbonyl group (AA6) and/or their carboxyl group (AA6 and **6**) (Fig. 12). The carboxyl groups of AA6 and **6** might be involved in H-bonds with S158 and R173, whose side chain could also establish a salt bridge with these compounds. Concerning the 2,6-dichlorophenyl ring, in compound AA6 this moiety is sandwiched between R363 and K290 which could form π-cation interactions with the ligand. Instead, in compound **6** this moiety is oriented towards SEPT6, and no relevant interactions were detected for the aromatic ring in this derivative. Interestingly, the docking pose of the active compound AA6 resembles the conserved experimental binding mode observed for GDP in human septins. Indeed, the aromatic ring of AA6 occupies the same region of the nucleotide purine core while one of the two carboxyl groups overlaps with the α-phosphate group of GDP (Fig. 12D).

Overall, our computational studies suggested that the engagement of Lys290, involved in the recognition of the physiological substrate and in the binding interface with SEPT6, by CM365 and AA6 might play a crucial role in the disruption of SEPT4 activity.

3.5. In vivo studies

3.5.1. CM365 inhibits lung metastasis dissemination in vivo

Since the metastatization process is accompanied by cytoskeletal changes [47,48], cell adhesion and invasion [9], on the basis of the *in vitro* results, the selected compound was assessed for its *in vivo* antimetastatic effects in a mouse model of lung experimental metastases using B16-F10 cells [27,49]. C57BL/6J mice were injected with B16-F10 cells in the tail vein in order to induce lung metastases and treated by i.p. injection with either CM365 (12.5 mg/kg) or vehicle for 21 days, sacrificed and subjected to complete necropsy [50]. To verify the therapeutic effect of our compound, the number of lung metastases were counted by ocular evaluation. As shown in Fig. 13A, CM365 treatment starting from the same day of B16-F10 cells injection (T0) significantly inhibited lung metastasis dissemination, compared to the control group. To further verify CM365 *in vivo* efficacy, another group of mice were treated 8 days after B16-F10 cells injection (T8). As shown in Fig. 13A, also in this treatment protocol CM365 induced a significant reduction in the number of lung metastases. Finally, we assessed the antimetastatic effect of our compound in association with the well-known chemotherapeutic agent paclitaxel. Interestingly, the co-treatment with CM365 from day 0 and paclitaxel on day 7 reduced the number of lung metastasis more efficiently than paclitaxel alone (Fig. 13A).

To monitor animal welfare during the CM365 treatment, the weight of the animals was checked at different days, and after sacrifice the weight of all their organs was registered; no severe adverse systemic effects were detected (Fig. 13B, Fig. S5).

Histological examination of the lung stained sections highlighted that CM365 treatment was able to counteract the development of *in vivo* metastatic melanoma cancer. Fig. 14 reports an overall slide acquisition, pinpointing the metastases with black circles. The control (CTR) group lungs were rich of metastases and the physiological structure of some lung lobes was totally lost (Fig. 14, left side of the panel). On the contrary, CM365 treated animals displayed substantially less metastases than CTR group, and the lung physiological structure was mostly maintained (Fig. 14, right side of the panel).

3.5.1.1. CM365 up-regulates IFN-γ and IL-1β and down-regulates IL-6 expression in vivo. In order to evaluate the cytokine expression pattern modulation by CM365 daily treatment, analysis of cytokine expression was assessed in the lung by real time PCR.

As shown in Fig. 15, CM365 altered the cytokine expression pattern, inducing an increase of IFN-γ and IL-1β and a reduction of IL-6

expression compared to the control group; while no significant effects were detected on TNF-α and IL-10 expression. No expression of IL-21 and IL-17A was detected in any sample.

4. Discussion

In a previous work, we studied the effects of the compound AA6 in a spontaneous lung metastasis mouse model of breast cancer, obtaining encouraging results, since AA6 prevented lung metastasis formation. At the cellular level AA6 was able to interfere with different downstream pathways involved in metastatic progression, i.e. metabolic alterations, inefficient DNA demethylation [11,19]. Starting from these observations, we decided to modulate the structure of AA6, in the search for more potent antimetastatic agents, together with the aim of identifying the structural elements crucial for its activity.

We first decided to modulate the succinic acid moiety. In compounds **7**, **8** and **9** the β-carboxylic group is lacking, all the three compounds showed a significant decrease in the maximal efficacy of B16-F10 cells invasiveness inhibition (45 ± 3 %, 39 ± 2 % and 41 ± 1 % respectively, *vs* 70 ± 4 % for AA6). Also, the substitution of the β-carboxylic acid group with a neutral alkyl chain (isopropyl, **2**) or with a basic substituent (imidazole, **3**; guanidine, **4**) caused a reduction of the *in vitro* maximal efficacy (Table 1). On the contrary, the introduction of an amide in place of the β-carboxylic acid group in compound **5** did not affect the inhibition of B16-F10 cells invasiveness, with a maximal efficacy of 65 ± 5 % and IC_{50} = 0.70 ± 0.4 μM, values similar to those obtained for compound AA6 (Table 1). Thus, in the position 3 of the succinic acid the presence of a substituent able to act as H-bond acceptor (HBA) seems to be preferred for the activity.

Afterwards, we investigated the importance of the configuration at the chiral carbon in position 2 of the succinic acid residue. The S-configuration (AA6) seems to be crucial, since the R-enantiomer **6** resulted inactive *in vitro*.

Then, we focused on the benzoylamino substituent; in particular, we first modified the distance between the diclorophenyl group and the amide carbonyl group, by inserting a one carbon or two carbon alkyl chain, obtaining compounds **12** and **13**, respectively. The insertion of the spacer between the benzene ring and the amide group did not significantly affect the *in vitro* activity with respect to AA6, since both **12** and **13** still showed a good maximal efficacy in inhibiting B16-F10 cells invasiveness (55 ± 5 % and 60 ± 4 %, respectively), and similar IC_{50} values (4.5 ± 3 μM and 2.4 ± 1 μM, respectively). Starting from these results, with the aim of obtaining a compound able to covalently bind to the target, we synthesized derivative **19** (CM365). Indeed, this compound, bearing a double bond activated by the close electron withdrawing carbonyl group, can lead to the formation of covalent adducts via Michael-type reactions with molecular targets, such as nucleophilic groups of functional or regulatory residues in proteins. CM365 maintained a good *in vitro* maximal efficacy of invasiveness inhibition, with an IC_{50} value slightly lower than AA6 (5.5 ± 3.8 μM *vs* 0.70 ± 0.10 μM, Table 1) and similar to those of **12** and **13**. We speculate that CM365 might behave as a targeted covalent inhibitor (TCI) being able to reach and bind the target, similarly to AA6, and then block the target through the formation of a covalent irreversible interaction. The inactivity of compound **18**, the dimethylester analogue of CM365, further demonstrated that the presence of carboxylic acid functionalities is necessary to establish interactions with the target and the presence of the electrophilic fragment alone is not sufficient to trigger the inhibitory effect on cell migration. Finally, with the scope of exploring the chemical space available for further substitution on the benzene ring of AA6, we also synthesized compound **11** bearing a supplementary phenyl ring in the *para* position. However, this substitution proved detrimental for the activity (Table 1).

To further demonstrate that our new molecules were able to interfere with the metastatic process, we tested the lead AA6 and CM365 for *in vitro* inhibition of B16-F10 cells migration and adhesion, which are two well-known initial steps of the metastatization process. For these studies, we chose the lead compound and its derivative CM365, in order to have two molecules with a good efficacy in *in vitro* invasiveness inhibition, but able to interact with the target in two different ways: a non-covalent interaction for AA6 and a predicted covalent interaction for CM365. The binding kinetics of a covalent inhibitor is different compared to that of a traditional non-covalent drug. Indeed, while non-covalent inhibitors efficacy and potency correlate with their affinity for the target (k_i), the efficacy and potency of covalent inhibitors mainly depend on their residence time (t_r), namely the time the drug remains bound to its target [22]. Both compounds were able to inhibit cell migration in the wound healing assay, even at low concentrations (Fig. 4); and both similarly inhibited B16-F10 cells adhesion to MS1 endothelial cells in a concentration-dependent manner (IC_{50} values = 0.16 ± 0.02 μM for AA6 and 0.086 ± 0.02 μM for CM365) (Fig. 5). These *in vitro* analyses suggest that both molecules may have similar efficacy in inhibiting the metastatic process.

In previous works [11,20], we characterized the downstream effects caused in the cells by AA6, but we did not identify its cellular target. To address this aspect, we started from the observation that AA6 increased cellular α-ketoglutarate (α-KG) levels in murine breast cancer 4 T1 cells [11]. Thus, we tested AA6 as an inhibitor of different isolated enzymes directly or indirectly involved in the regulation of α-KG, such as α-ketoglutarate dehydrogenase, succinate dehydrogenase, isocitrate dehydrogenase 1 R132H mutant, aspartate aminotransaminase [51–54]. None of these enzymes was significantly inhibited by AA6 (Table S3, Supplementary Material). The analysis of the intracellular fractions obtained from B16-F10 cells incubated with AA6 showed that no compound was detected, thus excluding an intracellular target and focusing our research on membrane proteins. On this basis, we thought that CM365 could be a promising tool in the search for the cellular target of our new antimetastatic agents. Indeed, the design and synthesis of a molecule able to form covalent adducts via Michael-type reactions with molecular targets offered us the chance to further investigate this aspect. We hypothesized that the covalent binding of CM365 might target a membrane protein and the membrane protein-CM365 adduct might be detected by a proteomic analysis. Covalent inhibitors are generally classified into two broad categories, according to whether the adducts with the protein targets are functionally reversible or not. Covalent reversible inhibitors bind to their target protein and subsequently dissociate from it at a rate that is faster than the turnover rate of the protein. On the other hand, covalent irreversible inhibitors form adducts to their protein targets that either do not dissociate from the protein during its lifetime or do so with a kinetic that is significantly longer than the re-synthesis rate of the protein. Covalent irreversible inhibitors most commonly employ Michael acceptors as the electrophilic warhead responsible for the binding to the desired target [22,55,56]. To be useful to our purposes, the CM365 covalent adduct with the target had to be irreversible; to verify this condition, we synthesized compound **25**, a biotinylated derivative of CM365. Compound **25**, although structurally bigger and bulkier, was able to inhibit B16-F10 cells invasiveness as well as CM365 (Table 1, Fig. 3), thus showing that biotinylation of CM365 did not interfere with the binding to the cellular target. The higher fluorescence measured in the membrane fractions isolated from B16-F10 cells incubated with **25**, washed, and finally incubated with the fluorescent tracer ExtrAvidin®-FITC, allowed us to confirm that the cellular target was actually a membrane protein and that the covalent bond with the target was irreversible as well. Then, we proceeded with the targeted identification of CM365 covalent protein adduct(s) by nLC-HR-MS/MS analysis of the membrane fractions isolated from B16-F10 cells incubated with CM365.

With the intent of localizing covalent adducts occurring on key residues of CM365 target membrane proteins, experimental MS spectra were processed by automatically searching for plausible mass shifts according to the speculated reaction mechanism (Proteome Discoverer software), and finally a target-based approach was used to clearly and

unambiguously identify the formation of the stable conjugate between CM365 and Septin-4 (Lys290).

Septins are a family of GTP-binding proteins that assemble into oligomeric complexes and polymers which main function is the spatial organization and compartmentalization of many cellular processes, including cytoskeletal assembly [57–60]. In particular, the four components of the cytoskeleton include: actin filaments, microtubules, intermediate filaments, and septin polymers. These cytoskeletal elements play crucial roles in mediating housekeeping and specialized functions in multiple cell types, i.e. regulation of cell shape and size, cell division, migration, cell–cell interactions, protein uptake and secretion, receptor signalling [61,62]. Moreover, septin remodeling is essential for the formation of cell membrane protrusions (microtentacles) in detached tumor cells [48,63]. Septins are localized to actin bundles or at the cytosol, or in particular for Septin-4, at the outer membrane of mitochondria [64], but it has been reported that septin self-assembly into filaments and higher-order structures occur by diffusion-driven annealing on the plasma membrane, and that detachment of cells causes redistribution of septins to the membrane, where microtentacle formation occurs [48]. Large septin filament arrays, stably interacting with the plasma membrane, may modify cortical morphogenesis by imposing membrane curvature, and affect the cortical rigidity of migrating cells, thus contributing to tumor metastasis [65]. Despite the lack of a recognizable transmembrane domain and other obvious membrane localization motifs, the association of septins with membranes has been attributed to a well characterized polybasic sequence residing between the *N*-terminal domain and the GTPase, typically about nine residues before the P-loop. This polybasic sequence is known to bind directly to phosphatidylinositol bisphosphate and phosphatidylinositol trisphosphate, and specifically confers membrane-binding capability to septin proteins [66].

With the aim to confirm that the antimetastatic effects of CM365 were mediated by its binding to septin-4, firstly we verified the presence of this protein in B16-F10 cells. Western blot analysis confirmed the presence of septin-4, and showed that the incubation with CM365 did not modify septin-4 expression in the cells (Fig. 9A). Subsequently, we decided to repeat the invasion assay in septin-4 lacking cells. U2OS cells were selected for the absence of septin-4, as shown by Liu [43] and here confirmed (Fig. 9B). Interestingly, the absence of septin-4 expression completely abrogated the CM365 inhibitory effect on cell invasiveness (Fig. S4).

Computational studies allowed us to further investigate the interaction of CM365 with its target. A model of SEPT4-SEPT6 dimer generated by homology modelling was employed for covalent docking analysis of the covalent adduct between Lys290 of SEPT4 and CM365. In Fig. 10 are reported the different residues involved in the interaction with the ligand, through salt bridge, H- and halogen bonds formation. The effect of the covalent adduct formation on the stability of SEPT4-SEPT6 dimer was investigated as well. The MD simulation highlighted that the CM365 covalent adduct induces multiple structural changes at the interface between the two proteins, which might be responsible for the inhibition of SEPT4 function (Fig. 11). The binding mode of derivatives AA6 and **6** was also investigated by docking simulation, in order to verify the SEPT4-binding capability of other compounds of the series. The docking study confirmed that the presence of substituents able to be involved in a network of H-bonds at the terminal position is important for the interaction with SEPT4. Indeed, the carboxyl group of AA6 and **6** can be involved in H-bonds with S158, T159 and R173 of SEPT4 (Fig. 12). In compound AA6, the 2,6-dichlorophenyl ring was also able to form π-cation interactions involving R363 and K290 with the protein, interactions that were not established by compound **6** (Fig. 12). Notably, CM365 was able to bind covalently to K290. This residue is conserved among septins and plays a role in substrate recognition as it is involved in interactions with the purine ring and the ribose moiety of GTP and GDP. In addition, crystallographic studies highlighted that in SEPT2, which belongs to the same subgroup of SEPT4, the corresponding lysine residue is implicated in the binding to SEPT6 [45]. Therefore, the contacts involving K290 appear to be crucial for the activity of these septin ligands as confirmed by the absence of activity for compound **6**.

On the basis of the good efficacy in inhibiting cell migration, the formation of covalent adducts and the identification of septin-4 as the target, we selected compound CM365 to be tested for its *in vivo* antimetastatic effects. No appropriate *in vitro* models are currently available that fully reproduce the complexity of *in vivo* metastasis dissemination [67]. For these reasons, we tested the *in vivo* activity of CM365 in a murine lung metastasis melanoma model [49,68]. The tested compound was able to reduce lung metastasis formation when the administration was started on the same day of B16-F10 cells injection; these results showed that CM365 was effective in the very early stages of the metastatic process. At the same time, CM365 efficacy was confirmed also starting its administration 8 days after melanoma cells injection (Fig. 13A), which suggests that CM365 was able to reduce lung metastasis establishment after the dissemination of the tumor cells. Finally, the strengthening effect induced by the co-administration of the cytotoxic agent paclitaxel together with CM365 is of great interest, being more effective than paclitaxel alone (Fig. 13A).

Noteworthy, *in vivo* treatment with CM365 modulated the immune response in the metastasized lungs, since it increased expression of IFN-γ and IL-1β and decreased expression of IL-6 (Fig. 15). The increased expression of IFN-γ is particularly interesting since this cytokine is produced by cytotoxic lymphocytes capable of anti-tumor activity. In this context the increased expression of IL-1β, that may have either pro- or anti-tumor effects in different tumors, might support the cytotoxic cell response in our highly immunogenic tumor model [69]. By contrast, the decreased expression of IL-6 may counteract metastases establishment since this cytokine has multiple pro-tumor activities [70]. These immunologic effects induced by CM365 treatment may depend on direct effects on immune cell migration, adhesion and granule secretion, which involve the cytoskeleton. Alternatively, they may be mediated by effects on the tumor cells, that are themselves capable to modulate the immune response. Certainly, further studies are required to deepen the immunological response triggered by CM365 administration and septin-4 binding.

5. Conclusions

The structural modulation of the lead compound AA6 performed in this work allowed us to obtain new compounds able to inhibit *in vitro* B16-F10 cell invasiveness, to draw some preliminary structure–activity relationship, and to obtain the new compound CM365 with *in vivo* antimetastatic effects. The identification of septin-4 as the most likely molecular target responsible of the downstream anti-metastatic effects observed, represents a good starting point for the future design of new derivatives. Moreover, targeting septin-4 with specific inhibitors to obtain new anti-metastatic agents could represent an innovative approach in the treatment of such a complex phenomenon. Finally, the encouraging results obtained by the co-administration of CM365 with paclitaxel in the inhibition of lung metastasis dissemination opens a broad horizon on the possible use of CM365 in combination with several drugs clinically used in cancer therapy.

CRediT authorship contribution statement

Federica Blua: Investigation. **Chiara Monge:** Investigation. **Simone Gastaldi:** Investigation. **Nausicaa Clemente:** Methodology, Investigation. **Stefania Pizzimenti:** Resources, Investigation. **Loretta Lazzarato:** Investigation. **Rebecca Senetta:** Investigation. **Serena Vittorio:** Investigation, Formal analysis. **Casimiro Luca Gigliotti:** Investigation. **Elena Boggio:** Writing – review & editing, Investigation. **Umberto Dianzani:** Writing – review & editing, Funding acquisition. **Giulio Vistoli:** Writing – review & editing, Methodology, Funding acquisition, Formal analysis.

Alessandra Anna Altomare: Writing – review & editing, Validation, Resources, Investigation, Formal analysis. **Giancarlo Aldini:** Writing – review & editing, Resources. **Chiara Dianzani:** Investigation, Funding acquisition. **Elisabetta Marini:** Writing – original draft, Visualization, Investigation, Funding acquisition, Conceptualization. **Massimo Bertinaria:** Writing – review & editing, Supervision, Project administration, Funding acquisition, Conceptualization.

Declaration of competing interest

The authors declare that they have no known competing financial interests or personal relationships that could have appeared to influence the work reported in this paper.

Acknowledgments

This work was supported by University of Turin, Ricerca Locale 2021, 2022 (BERM_RILO_21_01; MARE_RILO_22_01; DIAC_RILO_21_01; PZS_RILO_22_01; PZS_RILO_21_01) and IG20714 Associazione Italiana Ricerca sul Cancro, Milan Italy.

Appendix A. Supplementary data

Supplementary data to this article can be found online at https://doi.org/10.1016/j.bioorg.2024.107164.

References

[1] A. Chatterjee, E.J. Rodger, M.R. Eccles, Epigenetic drivers of tumourigenesis and cancer metastasis, Semin. Cancer Biol. 51 (2018) 149–159.
[2] M. Vizoso, H.J. Ferreira, P. Lopez-Serra, F.J. Carmona, A. Martínez-Cardús, M. R. Girotti, A. Villanueva, S. Guil, C. Moutinho, J. Liz, A. Portela, H. Heyn, S. Moran, A. Vidal, M. Martinez-Iniesta, J.L. Manzano, M.T. Fernandez-Figueras, E. Elez, E. Muñoz-Couselo, R. Botella-Estrada, A. Berrocal, F. Pontén, O. Jv, W. M. Gallagher, D.T. Frederick, K.T. Flaherty, U. McDermott, P. Lorigan, R. Marais, M. Esteller, Epigenetic activation of a cryptic TBC1D16 transcript enhances melanoma progression by targeting EGFR, Nat. Med. 21 (7) (2015) 741–750.
[3] G. Bergers, S.M. Fendt, The metabolism of cancer cells during metastasis, Nat. Rev. Cancer. 21 (3) (2021) 162–180.
[4] A.W. Lambert, D.R. Pattabiraman, R.A. Weinberg, Emerging biological principles of metastasis, Cell 168 (4) (2017) 670–691.
[5] S. Valastyan, R.A. Weinberg, Tumor metastasis: molecular insights and evolving paradigms, Cell 147 (2) (2011) 275–292.
[6] Y. Katsuno, S. Lamouille, R. Derynck, TGF-β signaling and epithelial-mesenchymal transition in cancer progression, Curr. Opin. Oncol. 25 (1) (2013) 76–84.
[7] B. De Craene, G. Berx, Regulatory networks defining EMT during cancer initiation and progression, Nat. Rev. Cancer. 13 (2) (2013) 97–110.
[8] J. Fares, M.Y. Fares, H.H. Khachfe, H.A. Salhab, Y. Fares, Molecular principles of metastasis: a hallmark of cancer revisited, Signal Transduct. Target Ther. 5 (1) (2020) 28.
[9] P. Katira, R.T. Bonnecaze, M.H. Zaman, Modeling the mechanics of cancer: effect of changes in cellular and extra-cellular mechanical properties, Front. Oncol. 3 (2013) 145.
[10] K. Ganesh, J. Massagué, Targeting metastatic cancer, Nat. Med. 27 (1) (2021) 34–44.
[11] S. Atlante, A. Visintin, E. Marini, M. Savoia, C. Dianzani, M. Giorgis, D. Sürün, F. Maione, F. Schnütgen, A. Farsetti, A.M. Zeiher, M. Bertinaria, E. Giraudo, F. Spallotta, C. Cencioni, C. Gaetano, α-ketoglutarate dehydrogenase inhibition counteracts breast cancer-associated lung metastasis, Cell Death Dis. 9 (7) (2018) 756.
[12] U.E. Martinez-Outschoorn, M. Peiris-Pagés, R.G. Pestell, F. Sotgia, M.P. Lisanti, Cancer metabolism: a therapeutic perspective. *Nat Rev Clin Oncol.* **2017**, (1): 11-31. Erratum in: *Nat Rev Clin Oncol.* **2017**, 14 (2):113.
[13] M.G. Vander Heiden, R.J. DeBerardinis, Understanding the intersections between metabolism and cancer biology, Cell 168 (4) (2017) 657–669.
[14] M.E. Figueroa, O. Abdel-Wahab, C. Lu, P.S. Ward, J. Patel, A. Shih, Y. Li, N. Bhagwat, A. Vasanthakumar, H.F. Fernandez, M.S. Tallman, Z. Sun, K. Wolniak, J.K. Peeters, W. Liu, S.E. Choe, V.R. Fantin, E. Paietta, B. Löwenberg, J.D. Licht, L. A. Godley, R. Delwel, P.J. Valk, C.B. Thompson, R.L. Levine, A. Melnick, Leukemic IDH1 and IDH2 mutations result in a hypermethylation phenotype, disrupt TET2 function, and impair hematopoietic differentiation, Cancer Cell 18 (6) (2010) 553–567.
[15] H. Zouridis, N. Deng, T. Ivanova, Y. Zhu, B. Wong, D. Huang, Y.H. Wu, Y. Wu, I. B. Tan, N. Liem, V. Gopalakrishnan, Q. Luo, J. Wu, M. Lee, W.P. Yong, L.K. Goh, B. T. Teh, S. Rozen, P. Tan, Methylation subtypes and large-scale epigenetic alterations in gastric cancer, Sci. Transl. Med. 4 (156) (2012) 156ra140.
[16] S.A. Mani, W. Guo, M.J. Liao, E.N. Eaton, A. Ayyanan, A.Y. Zhou, M. Brooks, F. Reinhard, C.C. Zhang, M. Shipitsin, L.L. Campbell, K. Polyak, C. Brisken, J. Yang, R.A. Weinberg, The epithelial-mesenchymal transition generates cells with properties of stem cells, Cell 133 (4) (2008) 704–715.
[17] S.M. Park, A.B. Gaur, E. Lengyel, M.E. Peter, The miR-200 family determines the epithelial phenotype of cancer cells by targeting the E-cadherin repressors ZEB1 and ZEB2. *Genes Dev.* **2008**, 22(7): 894-907. Erratum in: *Genes Dev.* **2009**, 23(11): 1378.
[18] Q.Q. Zhu, C. Ma, Q. Wang, Y. Song, T. Lv, The role of TWIST1 in epithelial-mesenchymal transition and cancers, Tumour Biol. 37 (1) (2016) 185–197.
[19] F. Spallotta, C. Cencioni, S. Atlante, D. Garella, M. Cocco, M. Mori, R. Mastrocola, C. Kuenne, S. Guenther, S. Nanni, V. Azzimato, S. Zukunft, A. Kornberger, D. Sürün, F. Schnütgen, H. von Melchner, A. Di Stilo, M. Aragno, M. Braspenning, W. van Criekinge, M.J. De Blasio, R.H. Ritchie, G. Zaccagnini, F. Martelli, A. Farsetti, I. Fleming, T. Braun, A. Beiras-Fernandez, B. Botta, M. Collino, M. Bertinaria, A.M. Zeiher, C. Gaetano, Stable oxidative cytosine modifications accumulate in cardiac mesenchymal cells from type2 diabetes patients: rescue by α-ketoglutarate and TET-TDG functional reactivation, Circ. Res. 122 (1) (2018) 31–46.
[20] R.R. Braeuer, I.R. Watson, C.J. Wu, A.K. Mobley, T. Kamiya, E. Shoshan, M. Bar-Eli, Why is melanoma so metastatic? Pigment Cell Melanoma Res. 27 (1) (2014) 19–36.
[21] F. van Zijl, G. Krupitza, W. Mikulits, Initial steps of metastasis: cell invasion and endothelial transmigration, Mutat. Res. 728 (1–2) (2011) 23–34.
[22] S. De Cesco, J. Kurian, C. Dufresne, A.K. Mittermaier, N. Moitessier, Covalent inhibitors design and discovery, Eur. J. Med. Chem. 138 (2017) 96–114.
[23] N.V. Mehta, M.S. Degani, The expanding repertoire of covalent warheads for drug discovery, Drug Discov Today. 28 (12) (2023) 103799.
[24] M. Cocco, G. Miglio, M. Giorgis, D. Garella, E. Marini, A. Costale, L. Regazzoni, G. Vistoli, M. Orioli, R. Massulaha-Ahmed, I. Détraz-Durieux, M. Groslambert, B. F. Py, M. Bertinaria, Design, synthesis, and evaluation of acrylamide derivatives as direct NLRP3 inflammasome inhibitors, ChemMedChem 11 (16) (2016) 1790–1803.
[25] D. Garella, S. Atlante, E. Borretto, M. Cocco, M. Giorgis, A. Costale, L. Stevanato, G. Miglio, C. Cencioni, E. Fernández-de Gortari, J.L. Medina-Franco, F. Spallotta, C. Gaetano, M. Bertinaria, Design and synthesis of N-benzoyl amino acid derivatives as DNA methylation inhibitors, Chem. Biol. Drug Des. 88 (5) (2016) 664–676.
[26] S. Gastaldi, V. Boscaro, E. Gianquinto, C.F. Sandall, M. Giorgis, E. Marini, F. Blua, M. Gallicchio, F. Spyrakis, J.A. MacDonald, M. Bertinaria, Chemical modulation of the 1-(Piperidin-4-yl)-1,3-dihydro-2H-benzo[d]imidazole-2-one scaffold as a novel NLRP3 inhibitor, Molecules 26 (13) (2021) 3975.
[27] C. Dianzani, C. Monge, G. Miglio, L. Serpe, K. Martina, L. Cangemi, C. Ferraris, S. Mioletti, S. Osella, C.L. Gigliotti, et al., Nanoemulsions as delivery systems for poly-chemotherapy aiming at melanoma treatment, Cancers 12 (2020) 1198.
[28] D. Marchis, A. Altomare, M. Gili, F. Ostorero, A. Khadjavi, C. Corona, G. Ru, B. Cappelletti, S. Gianelli, F. Amadeo, C. Rumio, M. Carini, G. Aldini, C. Casalone, LC-MS/MS identification of species-specific muscle peptides in processed animal proteins, J. Agric. Food Chem. 65 (48) (2017) 10638–10650.
[29] G. Baron, S. Borella, L. Della Vedova, S. Vittorio, G. Vistoli, M. Carini, G. Aldini, A. Altomare, An integrated metabolomic and proteomic approach for the identification of covalent inhibitors of the main protease (Mpro) of SARS-COV-2 from crude natural extracts, Talanta 252 (2023) 123824.
[30] A. Waterhouse, M. Bertoni, S. Bienert, G. Studer, G. Tauriello, R. Gumienny, F. T. Heer, T.A.P. de Beer, C. Rempfer, L. Bordoli, R. Lepore, T. Schwede, SWISS-MODEL: homology modelling of protein structures and complexes, Nucleic Acids Res. 46 (W1) (2018) W296–W303.
[31] UniProt Consortium, UniProt: the universal protein knowledgebase in 2021, Nucleic Acids Res. 49 (D1) (2021) D480–D489.
[32] R.A. Laskowski, M.W. MacArthur, D.S. Moss, J.M. Thornton, PROCHECK: a program to check the stereochemical quality of protein structures, J. Appl. Cryst. 26 (1993) 283–291.
[33] A. Pedretti, A. Mazzolari, S. Gervasoni, L. Fumagalli, G. Vistoli, The VEGA suite of programs: a versatile platform for cheminformatics and drug design projects, Bioinformatics 37 (8) (2021) 1174–1175.
[34] G. Jones, P. Willett, R.C. Glen, A.R. Leach, R. Taylor, Development and validation of a genetic algorithm for flexible docking, J. Mol. Biol. 267 (3) (1997) 727–748.
[35] D. Moi, S. Vittorio, A. Angeli, G. Balboni, C.T. Supuran, V. Onnis, Investigation on hydrazonobenzenesulfonamides as human carbonic anhydrase I, II, IX and XII inhibitors, Molecules 28 (1) (2022) 91.
[36] D.A. Case, T.E. Cheatham 3rd, T. Darden, H. Gohlke, R. Luo, K.M. Merz Jr, A. Onufriev, C. Simmerling, B. Wang, R.J. Woods, The Amber biomolecular simulation programs, J. Comput. Chem. 26 (16) (2005) 1668–1688.
[37] C. Tian, K. Kasavajhala, K.A.A. Belfon, L. Raguette, H. Huang, A.N. Migues, J. Bickel, Y. Wang, J. Pincay, Q. Wu, C. Simmerling, ff19SB: amino-acid-specific protein backbone parameters trained against quantum mechanics energy surfaces in solution, J. Chem. Theory Comput. 16 (1) (2020) 528–552.
[38] J. Wang, R.M. Wolf, J.W. Caldwell, P.A. Kollman, D.A. Case, Development and testing of a general amber force field. *J Comput Chem.* **2004**, 25(9): 1157-74. Erratum in: *J Comput Chem.* **2005**, 26(1): 114.
[39] M.J. Frisch, G.W. Trucks, H.B. Schlegel, G.E. Scuseria, M.A. Robb, J.R. Cheeseman, G. Scalmani, V. Barone, G.A. Petersson, H. Nakatsuji, X. Li, M. Caricato, A. V. Marenich, J. Bloino, B.G. Janesko, R. Gomperts, B. Mennucci, H.P. Hratchian, J. V. Ortiz, A.F. Izmaylov, J.L. Sonnenberg, D. Williams-Young, F. Ding, F. Lipparini, F. Egidi, J. Goings, B. Peng, A. Petrone, T. Henderson, D. Ranasinghe, V. G. Zakrzewski, J. Gao, N. Rega, G. Zheng, W. Liang, M. Hada, M. Ehara, K. Toyota, R. Fukuda, J. Hasegawa, M. Ishida, T. Nakajima, Y. Honda, O. Kitao, H. Nakai,

T. Vreven, K. Throssell, J.A. Montgomery Jr., J.E. Peralta, F. Ogliaro, M. J. Bearpark, J.J. Heyd, E.N. Brothers, K.N. Kudin, V.N. Staroverov, T.A. Keith, R. Kobayashi, J. Normand, K. Raghavachari, A.P. Rendell, J.C. Burant, S.S. Iyengar, J. Tomasi, M. Cossi, J.M. Millam, M. Klene, C. Adamo, R. Cammi, J.W. Ochterski, R.L. Martin, K. Morokuma, O. Farkas, J.B. Foresman, D.J. Fox, Gaussian 16, revision A.03, Gaussian Inc., Wallingford CT, 2016.
[40] D.R. Roe, T.E. Cheatham 3rd., PTRAJ and CPPTRAJ: software for processing and analysis of molecular dynamics trajectory data, J. Chem. Theory Comput. 9 (7) (2013) 3084–3095.
[41] T. Tubiana, J.C. Carvaillo, Y. Boulard, S. Bressanelli, TTClust: a versatile molecular simulation trajectory clustering program with graphical summaries, J. Chem. Inf. Model. 58 (11) (2018) 2178–2182.
[42] S. Vittorio, T. Seidel, A. Garon, R. Gitto, T. Langer, L. De Luca, In silico identification of potential druggable binding sites on CIN85 SH3 domain, Int. J. Mol. Sci. 22 (2) (2021) 534.
[43] W. Liu, SEPT4 is regulated by the Notch signaling pathway, Mol. Biol. Rep. 39 (4) (2012) 4401–4409.
[44] I.A. Cavini, D.A. Leonardo, H.V.D. Rosa, D.K.S.V. Castro, H. D'Muniz Pereira, N. F. Valadares, A.P.U. Araujo, R.C. Garratt, The structural biology of septins and their filaments: an update, Front. Cell Dev. Biol. 9 (2021) 765085.
[45] H.V. Dias Rosa, D.A. Leonardo, G. Brognara, J. Brandão-Neto, H. D'Muniz Pereira, A.P.U. Araújo, R.C. Garratt, Molecular recognition at septin interfaces: the switches hold the key, J. Mol. Biol. 432 (21) (2020) 5784–5801.
[46] B. Shuman, M. Momany, Septins from protists to people, Front. Cell Dev. Biol. 9 (2022) 824850.
[47] EMT, the cytoskeleton, and cancer cell invasion. Yilmaz M, Christofori G. *Cancer Metastasis Rev.* **2009**, 28(1-2): 15-33.
[48] K. Østevold, A.V. Meléndez, F. Lehmann, G. Schmidt, K. Aktories, C. Schwan, Septin remodeling is essential for the formation of cell membrane protrusions (microtentacles) in detached tumor cells, Oncotarget 8 (44) (2017) 76686–76698.
[49] W.W. Overwijk, N.P. Restifo, B16 as a mouse model for human melanoma. *Curr Protoc Immunol.* **2001**, Chapter 20: Unit 20.1.
[50] J. Yan, Z.Y. Wang, H.Z. Yang, H.Z. Liu, S. Mi, X.X. Lv, X.M. Fu, H.M. Yan, X. W. Zhang, Q.M. Zhan, Z.W. Hu, Timing is critical for an effective anti-metastatic immunotherapy: the decisive role of IFNγ/STAT1-mediated activation of autophagy, PLoS One 6 (9) (2011) e24705.
[51] C.M. Smith, J. Bryla, J.R. Williamson, Regulation of mitochondrial alpha-ketoglutarate metabolism by product inhibition at alpha-ketoglutarate dehydrogenase, J. Biol. Chem. 249 (5) (1974) 1497–1505.
[52] M. Xiao, H. Yang, W. Xu, S. Ma, H. Lin, H. Zhu, L. Liu, Y. Liu, C. Yang, Y. Xu, S. Zhao, D. Ye, Y. Xiong, K.L. Guan, Inhibition of α-KG-dependent histone and DNA demethylases by fumarate and succinate that are accumulated in mutations of FH and SDH tumor suppressors, Genes Dev. 26 (12) (2012) 1326–1338.
[53] S. Jones, J. Ahmet, K. Ayton, M. Ball, M. Cockerill, E. Fairweather, N. Hamilton, P. Harper, J. Hitchin, A. Jordan, C. Levy, R. Lopez, E. McKenzie, M. Packer, D. Plant, I. Simpson, P. Simpson, I. Sinclair, T.C. Somervaille, H. Small, G. J. Spencer, G. Thomson, M. Tonge, I. Waddell, J. Walsh, B. Waszkowycz, M. Wigglesworth, D.H. Wiseman, D. Ogilvie, Discovery and optimization of allosteric inhibitors of mutant isocitrate dehydrogenase 1 (R132H IDH1) displaying activity in human acute myeloid leukemia cells, J. Med. Chem. 59 (24) (2016) 11120–11137.
[54] J.M. Thornburg, K.K. Nelson, B.F. Clem, A.N. Lane, S. Arumugam, A. Simmons, J. W. Eaton, S. Telang, J. Chesney, Targeting aspartate aminotransferase in breast cancer, Breast Cancer Res. 10 (5) (2008) R84.
[55] J.M. Strelow, A perspective on the kinetics of covalent and irreversible inhibition. *SLAS Discov.* **2017**, 22(1): 3-20. Erratum in: *SLAS Discov.* **2017**, 22(5): 652.
[56] M. Bertinaria, S. Gastaldi, E. Marini, M. Giorgis, Development of covalent NLRP3 inflammasome inhibitors: chemistry and biological activity, Arch. Biochem. Biophys. 670 (2019) 116–139.
[57] E.T. Spiliotis, K. Nakos, Cellular functions of actin- and microtubule-associated septins, Curr. Biol. 31 (10) (2021) R651–R666.
[58] D. Angelis, E.T. Spiliotis, Septin mutations in human cancers, Front. Cell Dev. Biol. 4 (2016) 122.
[59] K.Y. Fung, L. Dai, W.S. Trimble, Cell and molecular biology of septins, Int. Rev. Cell Mol. Biol. 310 (2014) 289–339.
[60] B. Benoit, C. Poüs, A. Baillet, Septins as membrane influencers: direct play or in association with other cytoskeleton partners, Front. Cell Dev. Biol. 11 (2023) 1112319.
[61] A.I. Ivanov, H.T. Le, N.G. Naydenov, F. Rieder, Novel functions of the septin cytoskeleton: shaping up tissue inflammation and fibrosis, Am. J. Pathol. 191 (1) (2021) 40–51.
[62] L. Dolat, J.L. Hunyara, J.R. Bowen, E.P. Pauline Karasmanis, M. Elgawly, V. E. Galkin, E.T. Spiliotis, Septins promote stress fiber–mediated maturation of focal adhesions and renal epithelial motility, J. Cell Biol. 207 (2) (2014) 225–235.
[63] A.D. Weems, E.S. Welf, M.K. Driscoll, F.Y. Zhou, H. Mazloom-Farsibaf, B.J. Chang, V.S. Murali, G.M. Gihana, B.G. Weiss, J. Chi, D. Rajendran, K.M. Dean, R. Fiolka, G. Danuser, Blebs promote cell survival by assembling oncogenic signalling hubs, Nature 615 (7952) (2023) 517–525.
[64] Y. Mandel-Gutfreund, I. Kosti, S. Larisch, ARTS, the unusual septin: structural and functional aspects, Biol. Chem. 392 (8–9) (2011) 783–790.
[65] C. Poüs, L. Klipfel, A. Baillet, Cancer-related functions and subcellular localizations of septins, Front. Cell Dev. Biol. 4 (2016) 126.
[66] A. Bertin, M.A. McMurray, L. Thai, G. Garcia 3rd, V. Votin, P. Grob, T. Allyn, J. Thorner, E. Nogales, Phosphatidylinositol-4,5-bisphosphate promotes budding yeast septin filament assembly and organization, J. Mol. Biol. 404 (4) (2010) 711–731.
[67] O.F. Kuzu, F.D. Nguyen, M.A. Noory, A. Sharma, Current state of animal (mouse) modeling in melanoma research, Cancer Growth Metast. 8 (1) (2015) 81–94.
[68] E.E. Patton, K.L. Mueller, D.J. Adams, N. Anandasabapathy, A.E. Aplin, C. Bertolotto, M. Bosenberg, C.J. Ceol, C.E. Burd, P. Chi, M. Herlyn, S.L. Holmen, F. A. Karreth, C.K. Kaufman, S. Khan, S. Kobold, E. Leucci, C. Levy, D.B. Lombard, A. W. Lund, K.L. Marie, J.C. Marine, R. Marais, M. McMahon, C.D. Robles-Espinoza, Z. A. Ronai, Y. Samuels, M.S. Soengas, J. Villanueva, A.T. Weeraratna, R.M. White, I. Yeh, J. Zhu, L.I. Zon, M.S. Hurlbert, G. Merlino, Melanoma models for the next generation of therapies, Cancer Cell. 39 (5) (2021) 610–631.
[69] C. Rébé, F. Ghiringhelli, Interleukin-1β and Cancer, Cancers (basel). 12 (7) (2020) 1791.
[70] N. Kumari, B.S. Dwarakanath, A. Das, A.N. Bhatt, Role of interleukin-6 in cancer progression and therapeutic resistance, Tumour Biol. 37 (9) (2016) 11553–11572.